ADMET & DMPK 6(2) (2018) 105-139; doi: ***http://dx.doi.org/10.5599/admet.505***

Open Access : ISSN : 1848-7718

http://www.pub.iapchem.org/ojs/index.php/admet/index

Review

Cocrystal solubility-pH and drug solubilization capacity of sodium dodecyl sulfate – mass action model for data analysis and simulation to improve design of experiments

Alex Avdeef

in-ADME Research, 1732 First Avenue #102, New York, NY 10128 USA

E-mail: alex@in-adme.com; Tel.: +1-646-678-5713

Received: February 07, 2018; Revised: March 30, 2018; Available online: April 22, 2018

Abstract

This review discusses the disposition of the anionic surfactant, sodium dodecyl sulfate (SDS; i.e., sodium lauryl sulfate), to solubilize sparingly-soluble drugs above the surfactant critical micelle concentration (CMC), as quantitated by the solubilization capacity (k). A compilation of 101 published SDS k values of mostly poorly-soluble drug molecules was used to develop a prediction model as a function of the drug's intrinsic solubility, S_0, and its calculated H-bond acceptor/donor potential. In almost all cases, the surfactant was found to solubilize the neutral form of the drug. Using the mass action model, the k values were converted to drug-micelle stoichiometric binding constants, K_n, corresponding to drug-micelle equilibria in drug-saturated solutions. An in-depth case study (data from published sources) considered the micellization reactions as a function of pH of a weak base, B, (pK_a 3.58, S_0 52 µg/mL), where at pH 1 the BH.SDS salt was predicted to precipitate both below and above the CMC. At low SDS concentrations, two drug salts were predicted to co-precipitate: BH.Cl and BH.SDS. Solubility products of both were determined from the analysis of the reported solubility-surfactant data. Above the CMC, in a rare example, the charged form of the drug (BH^+) appeared to be strongly solubilized by the surfactant. The constant for that reaction was also determined. At pH 7, the reactions were simpler, as only the neutral form of the drug was solubilized, to a significantly lesser extent than at pH 1. Case studies also featured examples of solubilization of solids in the form of cocrystals. For many cocrystal systems studied in aqueous solution, the anticipated supersaturated state is not long-lasting, as the drug component precipitates to a thermodynamically stable form, thus lowering the amount of the active ingredient available for intestinal absorption. Use of surfactant can prevent this. A recently-described method for predicting the solubility product of cocrystals (coupled with predicted k values described here) allowed for simulations of solubility-pH speciation profiles of cocrystal systems in the presence of SDS. Well in advance of any actual measurements, these simulations can be used to probe conditions favorable to the design of cocrystal experiments where SDS stabilizes cocrystal suspensions against drug precipitation over a predicted range of pH values.

Keywords

drug-micelle binding constant; solubilization capacity; supersaturation; cocrystal solubilization; solubility-pH

Introduction

This review focuses on the pharmaceutical uses of sodium dodecyl sulfate (SDS; *i.e.*, sodium lauryl sulfate) to solubilize sparingly-soluble drugs by micellization. The mass action framework is used to describe drug-surfactant equilibria in drug-saturated suspensions as a function of pH. Examples applied to solids in cocrystal (CC) form are considered as part of a continuing interest in developing equilibrium simulation methods to identify optimal experimental conditions for cocrystal solubility-pH measurements.

For orally administered drugs which are poorly soluble in water, a number of formulation strategies can be used to improve their rate and extent of absorption [1]. For solid dosage forms, recent approaches have included the use of CC formulations [2-5]. Cocrystal suspensions can be stabilized using surfactants [6-9]. For liquid dosage forms (*e.g.*, soft gel capsules), surfactants are used to solubilize the active pharmaceutical ingredient (API) [10-12].

In standard dissolution measurements of poorly-soluble solids, some compounds initially show an enhanced release of the API, forming a supersaturated solution, which after a while results in the precipitation of the crystalline API ("*spring and parachute*" S&P effect). Cocrystals generally show such a tendency. A cocrystal is a composite of an uncharged API and an uncharged water-soluble "coformer" molecule (*e.g*., saccharin, nicotinamide, 4-aminobenzoic acid, *etc.*). As the API in the CC is released into an aqueous medium, a supersaturated solution is expected to form, with the maximum theoretical drug concentration called "cocrystal solubility," S_{CC} [5-9, 13, 14]. If sustained for a few hours, this enhanced concentration of the API can lead to increased oral absorption [15]. Compared to amorphous solids, which also form supersaturated solutions, CCs, being crystalline, are likely to have better long-term solid-state thermal, hygroscopic, and polymorphic stability [1-3].

The enhanced concentration of the API in CCs depends on the analytical concentrations of the two underlying components and on solution pH (in the case of ionizable components). Enhancement is not always sought: some cocrystals (*e.g.*, slow release formulations) are designed to produce a supersaturated solution with an initially *decreased* release of a water-soluble API ("*dive and surface*" D&S effect) [5,16,17].

However, the supersaturated state is not long-lasting for many CC systems studied in aqueous solution, given that the API (or coformer, as in the case of D&S) precipitates to a thermodynamically stable form, thus lowering (S&P) or raising (D&S) the concentration of the drug in solution. A way to overcome this API/coformer precipitation involves the use of surfactants [6-9].

A measure of the ability of the surfactant to solubilize a drug is referred to as solubilization capacity, often denoted by the symbol, k. It is defined as the number of moles of drug bound to the surfactant per mole of surfactant. As part of this study, 101 published SDS k values of mostly poorly-soluble drug molecules were gathered (Table 1). From these, a simple k prediction model was constructed, as a function of the API intrinsic solubility and hydrogen bond acceptor/donor potential.

Coupled with the *in silico* prediction of the k values, advantage was taken of the prediction of the solubility product, K_{sp}, of cocrystals [17], to simulate aqueous solution speciation as a function of pH, using a recently-described computational approach [16]. These simulation calculations can be used to probe conditions favorable to the design of cocrystal experiments where SDS is used to stabilize CC suspensions against precipitation of the API. Predictions can be extended to CCs whose solution thermodynamics had not been studied. Even drugs not known to form CCs can be tested against a series of coformer candidates. Examples are presented in the study to illustrate some of the possible uses of K_{sp} and k values.

Background – Drug Solubilization by Surfactants

Physicochemical Properties of Common Surfactants

Surfactants are surface-active molecules which contain a hydrophobic region and a hydrophilic head group. Such amphiphilic molecules dissolve in aqueous solution in ways that minimize contact between water and hydrophobic parts of the surfactant. This lowers the free energy of solvation. At low concentrations these molecules tend to accumulate at the boundaries between two phases, such as the air-water interface, where the hydrophobic groups position on the airside. Solid-liquid interfaces may also be sites of adsorption (*e.g.*, vessel walls, filter barriers, undissolved drug solids, *etc.*). Such available interfacial sites reach saturation as the surfactant concentration is increased up to the "critical micelle concentration" (CMC). Above the CMC, unattached surfactant monomers begin to self-associate to form spheroidal aggregates ("micelles") in the bulk aqueous solution, with hydrophobic portions of the surfactant positioning in the core of the micelle and hydrophilic parts forming a shell around the micelle body. Micelles may consist of 50-100 or more surfactant molecules. The CMC is detected as the point corresponding to the maximum change in the gradient of a particular property (*e.g.*, surface tension, conductivity, osmotic pressure, drug-micelle binding, surfactant monomer and counterion concentrations, *etc*.) vs. total surfactant concentration. On further increases in concentration above the CMC, the monomer concentration more or less plateaus while the micelle aggregates continue to increase in number but generally not in size. These micelle bodies are capable of encapsulating drug molecules. Poorly-soluble apolar drugs are drawn into the core of the micelle. Charged or polar amphiphilic drugs can position nearer the water-micelle surface.

Sodium Dodecyl Sulfate (SDS)

Sodium dodecyl sulfate (SDS) is a common anionic surfactant. It is an ester of sulfuric acid, comprising a single aliphatic C_{12} chain (structure in Fig. 1a). Since the pK_a is near zero, the SDS monomer is practically fully ionized in water. The surfactant is generally introduced into the aqueous solution as the sodium salt. Many of the physicochemical properties of SDS are well characterized [11, 12, 18-20]. It is considered to be a safe excipient in tablet or capsule formulations. In water, SDS forms nearly monodispersed micelles with the approximate aggregation number, N_{agg} = 62. At 25 °C the CMC is 8.3 mM in water (value varies somewhat, depending on the determination method [18, 19]). Solubilization of drugs can alter the CMC [12]. The negative charge of the 62-SDS micelle is approximately 80 % neutralized by about 50 sodium counterions, electrostatically held in the Stern layer comprising the outer shell of the spherical micelle [11]. Above the CMC, the solutions consist of SDS^- monomers and mainly $SDS_{62}Na_{50}^{12-}$ aggregates.

Effective Charge on SDS Micelles

The degree of counterion dissociation in Q_m-charged SDS micelles, $\alpha = (N_{agg} - Q_m)/N_{agg}$, is (i) not expected to be greatly affected by moderate temperature changes, (ii) not affected by solubilization of small organic solutes, (iii) only slightly dependent on the SDS concentration, and (iv) strongly affected by the type and concentration of counterion [12]. Increasing ionic strength is expected to lower α (*i.e.*, making the micelles less charged). In the computations here, the approximation is made that α and N_{agg} are constants (*i.e.,* micelles are assumed to be $SDS_{62}Na_{50}^{12-}$).

Mass Action Equilibrium Model for Sodium Dodecyl Sulfate (SDS)

In the mass action treatment of the micelle formation, sodium ions, monomers, and micelles are in equilibrium, according to the cumulative expression below (assuming the above metrics).

$$62\ SDS^- + 50\ Na^+ \leftrightarrows SDS_{62}Na_{50}^{12-} \qquad K_{SDS} = [SDS_{62}Na_{50}^{12-}] / [SDS^-]^{62}[Na^+]^{50} \qquad (1)$$

Figure 1 shows the simulation results based on Eq. (1), where the species in solution were calculated, as a function of added total surfactant concentration, using the program *p*DISOL-X (*cf*., below).

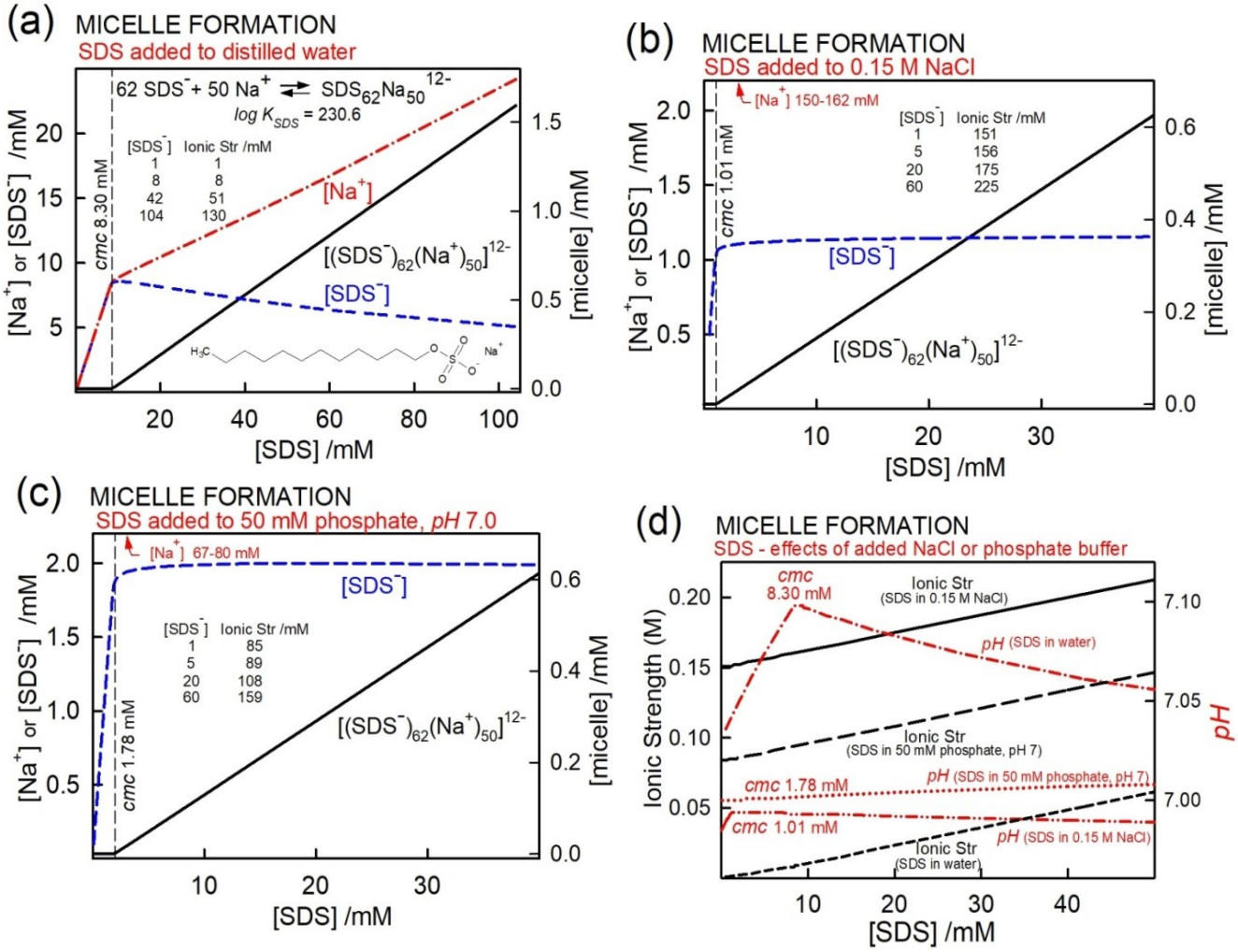

Figure 1. Simulation of formation of SDS micelles. Sodium dodecyl sulfate added to (a) distilled water, (b) 0.15 M NaCl solution, and (c) pH 7 solution of 50 mM phosphate. Ionic strength and pH change as concentration of surfactant is increased (d). See text.

In frame (a), simulation with aggregation constant log K_{SDS} = 230.6 results in CMC = 8.30 mM. The K_{SDS} constant was systematically varied in the calculations until the target CMC was obtained. As the surfactant concentration is increased in the simulation, SDS^- and Na^+ ions are released in equal concentrations, until the CMC value is reached. With further increases in surfactant concentration, the [SDS^-] and [Na^+] concentrations become unequal: that of the monomer *decreases,* as that of the counterion increases, due to the 62:50 stoichiometry of the micelles formed. The ionic strength changes over a broad range, increasing from 1 to 130 mM as the surfactant concentration is taken from 1 to 104 mM, which has an impact on the K_{SDS} binding constant and the pH of the solution (since electrode calibration parameters depend on ionic strength; *cf.*, Fig. 1d).

In frame (b), the surfactant is added to a 0.15 M NaCl solution. Using the same K_{SDS} constant, the CMC is predicted to decrease from 8.30 to 1.01 mM. The ionic strength increases over a narrow range, 151-225 mM, as the surfactant increases in concentration from 1 to 60 mM. In the background of higher ionic strength, the [SDS^-] concentration remains relatively constant at 1.01 mM (the CMC value), as the

surfactant concentration is increased above the CMC. The $[Na^+]$ concentration (off-scale) remains nearly constant, at 150-162 mM.

In frame (c), the surfactant is added to a 50 mM solution of phosphate buffer at pH 7. Using the same K_{SDS} in the calculation, CMC = 1.78 mM. The ionic strength, which is intermediate between that of the above two cases (*cf.*, Fig. 1d), clearly affects the CMC. A linear regression of the above three values of log CMC vs. ionic strength (I_{CMC}, evaluated at the CMC) produces: log CMC = -3.56 - 0.73 log I_{CMC}.

A similar relationship, experimentally-determined by Fuguet *et al.* [18], is log CMC = - 3.23 - 0.49 log C_i, where C_i is the added counterion concentration (about 1.5 times the phosphate concentration). Fuguet *et al.* used three different methods to measure CMC. In distilled water, the measured CMC = 8.08 ± 0.12mM; in 50 mM phosphate buffer (pH 7) CMC = 1.99 ± 0.02 mM [18]. These measured values are remarkably similar to those derived by purely *in silico* mass action simulations with the aggregation constant log K_{SDS} = 230.6. The mass action model could be used to try to predict many of the factors that make CMC value different from that found in water, such as type and amount of electrolytes, ionic strength, buffer pH, temperature, and added drugs. Some examples of this will be explored below.

In the simulations, it was found that pH could be used to indicate CMC, as shown in Figure 1d for the pure water case (dash-dot curve). The figure also indicates that the ionic strength increases nearly linearly with total surfactant added. The *p*DISOL-X calculation adjusts both equilibrium constants and pH electrode calibration parameters for changes in ionic strength.

Molar Solubilization Capacity (ℵ) and the Drug-Micelle Binding Constant, K_n

The solubilization capacity (ℵ) of a sparingly-soluble drug can be simply measured. The observed total solubility of the drug is plotted against the total added surfactant concentration. For $[SDS]_{tot}$ > CMC, the curve is usually linear: the slope in this region is the ℵ value.

As a simplified example of the mass action methodology, consider the following chemical equilibria involving SDS and a basic drug, B, which has a single pK_a, well below 7. Consider also that enough surfactant is added to water that $[SDS]_{tot}$ > CMC. The total micelle concentration, $[mic]_{tot} = ([SDS]_{tot} - CMC)/N_{agg}$.

$$BH^+ \leftrightarrows B + H^+ \qquad K_a = [B][H^+] / [BH^+] \qquad (2)$$

$$nB + mic^{12-} \leftrightarrows B_nmic^{12-} \qquad K_n = [B_nmic^{12-}] / [B]^n[mic^{12-}] \qquad (3)$$

$$B(s) \leftrightarrows B \qquad S_0 = [B] \qquad (4)$$

K_n is the drug-micelle binding constant, where n refers to the number of drug molecules bound to a micelle, and S_0 Is the intrinsic solubility of the drug (*cf.*, Glossary).

If the concentration of the drug is kept below its intrinsic solubility, then Eq. (4) need not be considered. In such a homogeneous micellar solution, the three independent reactants are B, mic^{12-}, and H^+. The corresponding mass balance equations may be stated as:

$$[B]_{tot} = [B] + [BH^+] + n[B_nmic^{12-}] \qquad (5)$$

$$[mic]_{tot} = [mic^{12-}] + [B_nmic^{12-}] \qquad (6)$$

$$[H]_{tot} = [H^+] - K_w / [H^+] + [BH^+] . \qquad (7)$$

K_w is the ionization constant of water. Eq. (7) is the hydrogen excess, which can be negative in alkaline solutions. On substituting the equilibrium quotients from Eqs. (2) and (3) into the mass balance equations,

one gets three polynomials as a function of the three reactants (B, mic^{12-}, and H^+) and the equilibrium constants K_a, K_w, and K_n.

$$[B]_{tot} = [B] + [B][H^+]/K_a + nK_n [B]^n [mic^{12-}] \quad (8)$$

$$[mic]_{tot} = [mic^{12-}] + K_n [B]^n [mic^{12-}] \quad (9)$$

$$[H]_{tot} = [H^+] - K_w / [H^+] + [B][H^+]/K_a \ . \quad (10)$$

The [B], $[mic^{12-}]$, and $[H^+]$ roots of the above equations, as well as the K_n constant, are solved using standard mathematical techniques [16, 17]. K_w and K_a are generally provided as fixed parameters in the calculation.

If the drug precipitates in the micellar medium, then the calculation needs to incorporate Eq. (4), as described in detail elsewhere [16]. In the aqueous-micellar-solid medium Eq. (8) defines the total solubility as a function of pH and the extent of drug-micelle binding, with [B] = S_0.

$$\begin{aligned} S_{tot} &= S_0 (1 + 10^{-pH + pKa}) + nK_n S_0^n [mic^{12-}] \\ &= S_0 (1 + 10^{-pH + pKa}) + nK_n S_0^n /(1 + K_n S_0^n) [mic]_{tot} \\ &= S_0 (1 + 10^{-pH + pKa}) + nK_n S_0^n /(1 + K_n S_0^n) \{ [SDS]_{tot} - CMC \}/N_{agg} \ . \end{aligned} \quad (11)$$

For $[SDS]_{tot}$ > CMC, the first derivative $dS_{tot}/d[SDS]_{tot}$ of the above equation defines κ.

$$\begin{aligned} \kappa &= n K_n S_0^n / \{ (1 + K_n S_0^n) N_{agg} \} \\ &= n f_{bm} / N_{agg} \\ &= N_d / N_{agg} \end{aligned} \quad (12)$$

The bound-micelle fraction, $f_{bm} = [B_n mic^{12-}]/[mic]_{tot} = K_n S_0^n /(1 + K_n S_0^n)$, which can take on values 0-1. From this, the average number of bound drugs per *micelle* is $N_d = n f_{bm}$. Eq. (12) indicates that κ is a function of both the intrinsic solubility, S_0, and the drug-micelle binding constant, K_n. If both κ and S_0 are known, or can be *in silico* estimated, then one can calculate from Eq. (12) the drug-micelle binding constant as:

$$\log K_n = \log \kappa - n \log S_0 + \log N_{agg} - \log (n - \kappa N_{agg}) \ . \quad (13)$$

A single value of n implies a perfectly monodisperse distribution of micelle size. A narrow range of n values is more likely to reflect the actual equilibrium process, but the calculation model considered here assumed a single value. If the total solubility, Eq. (11), is the only dependent variable in the design equation to determine K_n by regression analysis, then any practical value of $n > \kappa N_{agg}$ would satisfy the fitting process. In the discussion here, n is taken to be κN_{agg} rounded up to the next integral value (using the modulo operator), *i.e.,*

$$n = 1 + \kappa N_{agg} - mod(\kappa N_{agg}, 1) \ . \quad (14)$$

Note that Eq. (13) is only valid for solubilization of uncharged drugs (*e.g.*, Eq. 3), where the only precipitate in the suspension is the nonionized drug. A different explicit equation can be derived to take into account charged-drug precipitation and SDS solubilization of charged drug (not done here).

Equilibrium Model and the Computer Program

The general computer program *p*DISOL-X (*in-ADME* Research) was used to solve mass balance expressions, such as Eqs. (8)-(10), for all of the reactant concentrations in both aqueous and the aqueous-micellar-solid media. The program can analyze single-API solubility data [21-25] or cocrystal dual-

concentration eutectic data, as a function of pH [16, 17]. Salt solubility products (including drug-SDS salt formation), complexation reactions (*e.g.*, drug-micelle binding), and aggregation formations (drug or surfactant) can be considered. Algorithms for temperature [26] and automatic ionic strength [27] compensations have been incorporated. During calculation, the equilibrium constants are adjusted for activity effects, based on the Stokes-Robinson hydration theory [21]. The overall generalized approach allows for quick testing of many possible equilibrium models.

The details of how the solubility products are determined by regression analysis of eutectic data and how simulation calculations are performed using the K_{sp} and other equilibrium constants are not presented here, since that procedure already has been described in substantial depth elsewhere [16, 17]. Briefly, the equilibrium analysis does not depend on explicitly-derived extensions of the Henderson-Hasselbalch solubility equations, such as Eq. (11). The computational algorithm derives its own implicit equations internally in the context of the mass action model, given a set of equilibria (entered as text arrays, with hash tags denoting solid phase: *e.g.*, Eqs. (2)-(4) with n=2, "B+H=BH", "2B+mic=B2mic", and "B=B#") and the corresponding estimated equilibrium constants. The text array of equilibria is automatically parsed to construct the appropriate mass balance expressions in terms of reactant concentrations and equilibrium constants. The weighted nonlinear least-squares calculation considers the contribution from multiple substances – not only the API, micelle, and coformer, but also all of the reactants in solution, including buffers and background salts used to control the ionic strength. Currently, up to three solid phases may be addressed in the same calculation (provided they do not violate the Gibbs' Phase Rule constraint, for which the computer program tests). In cocrystal applications, the procedure treats the measured total aqueous API and coformer equilibrium concentrations, $[API]_{tot}$ and $[cof]_{tot}$, as dependent variables (*cf.*, Appendix). The surfactant concentration, reactant weights, reagent volumes, and pH are treated as independent variables, whereas the equilibrium constants are the potentially refinable parameters.

Data Sources

Molar Solubilization Capacity, $\Bbbk$

The 101 $\Bbbk$ values used in this study were gathered from published sources [28-53], and are listed in Table 1. In most of the studies, multi-point aqueous-micellar-solid solubility-SDS data were displayed solely in plots. These plots were digitized here using WebPlotDigitizer v.3.5 (https://automeris.io/WebPlotDigitizer/), from which the $\Bbbk$ values were re-determined, not only to corroborate the published $\Bbbk$ values, but also to determine the extent of nonlinearity in the [SDS] > CMC data. In several cases with high SDS concentrations, the slopes slightly decreased with increasing surfactant concentration. The re-calculated $\Bbbk$ values were equated to the slopes evaluated at the CMC. Not all values could be re-calculated. For example, the calculated $\Bbbk$ values of iminophenazines (including clofazimine) studied by Fahelelbom *et al.* [30] were taken directly from a plot; details of their determination were not reported in the publication. In just one instance, the $\Bbbk$ values were calculated from aqueous micellar systems (without drug precipitate): Garrone *et al*. [31] reported SDS-water partition coefficients, $P_{SDS\text{-}water}$, for a series of benzoic acid derivatives, determined from shifts in the pK_a values as a function of the SDS added. Calculated $\Bbbk = P_{SDS\text{-}water} \cdot S_0 \cdot V_m / (1 - [SDS]_{tot} \cdot V_m)$ [12], where the partial molar volume of SDS, V_m, was taken to be 0.26 M^{-1} [31].

Intrinsic Solubility S_0 Constants

Drug intrinsic solubility values (S_0) were taken from the literature, averaged where replicate sources

were available [17, 55, 56]. Most of the reported values (*e.g.*, in the *Handbook of Aqueous Solubility Data* [54]) have been published as concentrations (S_w) in saturated aqueous solutions of the drug, added in the neutral form to unbuffered water. Table 1 lists the log S_0, adjusted for the assay temperature [26].

Ionization Constants (pK_a)

The pK_a values used here (Table 1) were taken from the Wiki-pK_a database: http://www.in-adme.com/wiki_pka.php/. Literature pK_a values are often reported at 25 °C and 0.15 M ionic strength. When the assay temperature or ionic strength were different from literature conditions, pK_a values were adjusted to match the experimental conditions, using Stokes-Robinson hydration theory [21] for ionic strength [16, 27] and an empirical method for temperature [57] effects.

Examples of Published Solubility-SDS Data

Figures 2-7 illustrate drug multi-point solubility as a function of SDS concentration, with molecules grouped according to acid-base characteristics. In the figures, frames contain the structure of the molecule considered, and indicate assay temperature, solution makeup (distilled water, or buffer type and pH, or whether background salt had been added), equilibration times, pK_a (acids underlined), log S_0, and log P_{oct} constants. Each curve comprises a horizontal region ([SDS] < CMC) and a region of increasing solubility ([SDS] > CMC). The points in the latter region were selected for linear/curvilinear regression. The solid red curves are the connections of two curves: the regression-fitted curve and the horizontal lines where solubility is not appreciably affected by SDS. At the intersection of these curves (indicated by arrows) are concentrations which may be taken as the CMC values. The slopes of the curves in the [SDS] > CMC region were taken to be the k values (Table 1) and are indicated in units of mol_{drug}/mol_{SDS}. In cases the curves were nonlinear, a parabolic fit was used, and the indicated slopes were evaluated at [SDS] = CMC.

Table 1. Drug solubilization capacity (k) and other physicochemical parameters [a]

Compound	Type	pK_a (acid)	pK_a (base)	t(`C)	k (calc) [b]	k (obs) [c]	± SD	N [d]	log K_n [e]	n	f_{bm}	N_d	log P_{oct}	log S_0	±SD	N	$\Sigma\alpha_2^H$	$\Sigma\beta_2^H$	π_2	R_2	V_x	Comments	Ref
Artemisinin	N			22	0.191	**0.191**	0.013	11	45	12	0.99	11.8	2.90	-3.61	0.01	1	0.00	1.27	1.96	1.11	2.04		[28]
Atazanavir	B		4.52	37	0.017	**0.0056**	0.0002	9	5.3	1	0.35	0.35	4.54	-5.53	0.41	2	1.14	3.90	5.10	3.54	5.59		[29]
B3640 (iminophenazine)	B		8.09	37	0.00258	**0.00040**			5.4	1	0.025	0.025	3.58	*-7.04*			0.32	1.71	2.61	3.85	3.87		[30]
B3770 (iminophenazine)	B		8.80	37	0.00050	**0.00024**			6.5	1	0.015	0.015	4.78	*-8.35*			0.19	1.74	2.64	3.86	4.15		[30]
B3785 (iminophenazine)	B		8.60	37	0.00084	**0.00028**			6.2	1	0.018	0.018	4.39	*-7.94*			0.19	1.73	2.64	3.86	4.01		[30]
B628 (iminophenazine)	B		8.48	37	0.00283	**0.00070**			5.6	1	0.043	0.043	3.31	*-6.97*			0.19	1.23	2.39	3.6	3.03		[30]
B826 (iminophenazine)	B		8.81	37	0.00060	**0.00027**			6.4	1	0.017	0.017	4.50	*-8.21*			0.19	1.76	2.55	3.65	4.12		[30]
Benzoic Acid	A	3.96		35	1.038	**0.769**	0.0473	6	71	48	0.99	47.7	1.87	-1.44	0.04	13	0.57	0.44	1.08	0.75	0.93		[31]
Benzoic Acid,3-Cl-	A	3.82		35	0.359	**0.266**	0.0258	6	43	17	0.97	16.5	2.70	-2.43	0.20	1	0.64	0.44	1.16	0.90	1.05		[31]
Benzoic Acid,3-F-	A	3.86		35	0.620	**0.408**	0.0234	6	50	26	0.97	25.3	2.15	-1.86	0.20	1	0.64	0.45	1.04	0.67	0.95		[31]
Benzoic Acid,3-HO-	A	4.09		35	0.672	**1.486**	0.2163	6	102	93	0.99	92.1	1.49	-1.08	0.04	4	1.06	0.72	1.29	0.98	0.99		[31]
Benzoic Acid,3-NO2-	A	3.40		35	0.781	**0.870**	0.1656	6	91	54	0.99	54.0	1.82	-1.62	0.09	6	0.64	0.54	1.65	1.02	1.11		[31]
Benzoic Acid,4-Br-	A	3.98		35	0.128	**0.034**	0.0029	5	11	3	0.71	2.1	2.85	-3.47	0.16	2	0.66	0.44	1.24	1.08	1.11		[31]
Benzoic Acid,4-Cl-	A	3.84		35	0.177	**0.056**	0.0029	6	13	4	0.87	3.5	2.74	-3.13	0.20	1	0.66	0.44	1.16	0.90	1.05		[31]
Benzoic Acid,4-CN-	A	3.48		35	0.578	**0.318**	0.0548	6	40	20	0.98	19.7	1.56	-1.90	0.20	1	0.66	0.59	1.56	0.92	1.09		[31]
Benzoic Acid,4-HO-	A	4.32		35	0.646	**0.222**	0.0161	6	19	14	0.98	13.8	1.57	-1.22	0.10	6	1.00	0.72	1.29	0.98	0.99		[31]
Benzoic Acid,4-MeO-	A	4.44		35	0.325	**0.069**	0.0040	6	14	5	0.85	4.3	1.95	-2.65	0.03	2	0.57	0.66	1.17	0.81	1.13		[31]
Benzoic Acid,4-NO2-	A	3.31		35	0.290	**0.107**	0.0159	6	20	7	0.95	6.6	1.89	-2.62	0.20	1	0.66	0.54	1.65	1.02	1.11		[31]
Carbamazepine	N			37	0.346	**0.339**		3	68	22	0.96	21.0	2.45	-3.03	0.17	13	0.39	0.92	2.06	2.12	1.81		[32]
Carbamazepine	N			25	0.312	**0.314**	0.003	4	66	20	0.97	19.4	2.45	-3.21	0.17	13	0.39	0.92	2.06	2.12	1.81	dihydrate	[33]
Carbamazepine	N			25	0.312	**0.313**	0.007	4	66	20	0.97	19.4	2.45	-3.21	0.17	13	0.39	0.92	2.06	2.12	1.81	CC (nicrotinamide)	[33]
Carbamazepine	N			25	0.312	**0.309**	0.025	4	66	20	0.96	19.2	2.45	-3.21	0.17	13	0.39	0.92	2.06	2.12	1.81	CC (mixture)	[33]
Carbamazepine	N			25	0.312	**0.298**	0.007	11	63	19	0.97	18.5	2.45	-3.21	0.17	13	0.39	0.92	2.06	2.12	1.81	CC (4-NH_2-benzoic acid), *pH* 4.0	[6]
Carbamazepine	N			25	0.312	**0.348**	0.017	7	72	22	0.98	21.6	2.45	-3.21	0.17	13	0.39	0.92	2.06	2.12	1.81	CC (saccharin), pH 2.2	[6]

Table 1. Continued…

Compound	Type	pK_a (acid)	pK_a (base)	t(`C)	k_e (calc) [b]	k_e (obs) [c]	± SD	N [d]	log K_n [e]	n	f_{bm}	N_d	log P_{oct}	log S_0	±SD	N	$\Sigma\alpha_2^H$	$\Sigma\beta_2^H$	π_2	R_2	V_x	Comments	Ref
Carbamazepine	N			25	0.312	**0.334**	0.055	5	69	21	0.99	20.7	2.45	-3.21	0.17	13	0.39	0.92	2.06	2.12	1.81	CC (salicylic acid), pH 3.0	[6]
Carbamazepine	N			25	0.312	**0.297**	0.007	10	63	19	0.97	18.4	2.45	-3.21	0.17	13	0.39	0.92	2.06	2.12	1.81	CC (succinic acid), pH 3.1	[6]
Carbendazim	AB	10.52	4.48	23	0.092	**0.079**	0.012	4	24	5	0.98	4.9	1.52	-4.47	0.03	3	0.71	0.99	1.86	1.64	1.36		[34]
Carvedilol	B		7.75	37	0.020	**0.051**	0.001	5	22	4	0.79	3.2	4.14	-5.40	0.36	7	0.62	2.09	3.00	3.08	3.10	pH 1.2	[35]
Carvedilol	B		7.75	37	0.020	**0.061**	0.002	5	23	4	0.94	3.8	4.14	-5.40	0.36	7	0.62	2.09	3.00	3.08	3.10	pH 3.0	[35]
Carvedilol	B		7.75	37	0.020	**0.064**	0.005	5	23	4	0.99	3.9	4.14	-5.40	0.36	7	0.62	2.09	3.00	3.08	3.10	pH 4.5	[35]
Carvedilol	B		7.75	37	0.020	**0.061**	0.006	5	23	4	0.94	3.8	4.14	-5.40	0.36	7	0.62	2.09	3.00	3.08	3.10	pH 5.8	[35]
Carvedilol	B		7.75	37	0.020	**0.063**		5	23	4	0.98	3.9	4.14	-5.40	0.36	7	0.62	2.09	3.00	3.08	3.10	pH 6.8	[35]
Carvedilol	B		7.75	37	0.020	**0.061**	0.001	5	23	4	0.94	3.8	4.14	-5.40	0.36	7	0.62	2.09	3.00	3.08	3.10	pH 7.2	[35]
Clofazimine	B		8.51	37	0.0012	**0.0006**			6.2	1	0.039	0.039	4.40	-7.63	0.02	1	0.19	1.28	2.34	3.50	3.45		[30]
Curcumin	A	10.51 9.88 8.37		22	0.003	**0.027**	0.001	9	16	2	0.82	1.6	2.85	-7.52	0.20	1	0.55	1.67	2.85	2.30	2.77		[28]
Diazepam	B		3.41	24	0.146	**0.349**	0.014	3	85	22	0.98	21.6	2.99	-3.81	0.11	10	0.00	1.04	1.72	2.11	2.07		[36]
Diazepam	B		3.41	24	0.146	**0.261**	0.003	3	66	17	0.95	16.2	2.99	-3.81	0.11	10	0.00	1.04	1.72	2.11	2.07	0.15M NaCl	[36]
Erythromycin	B		8.82	25	0.546	**0.345**	0.117	4	62	22	0.97	21.4	2.54	-2.75	0.26	4	1.05	4.63	3.04	2.51	5.77		[37]
Estradiol,17β-	A	4.25		24	0.029	**0.022**	0.002	3	10	2	0.69	1.4	3.86	-4.90	0.18	4	0.81	0.95	2.30	1.85	2.20		[36]
Fenofibrate	N			25	0.061	**0.035**	0.008	4	18	3	0.72	2.2	5.23	-5.90	0.32	5	0.00	1.13	2.11	1.62	2.72		[38]
Glibenclamide	A	5.30		25	0.0065	**0.00047**	0.0002	1	5.0	1	0.029	0.029	3.75	-6.54	0.44	10	0.85	2.01	3.84	2.64	3.47		[39]
Glibenclamide	A	5.30		25	0.0065	**0.00089**	0.001	1	5.3	1	0.055	0.055	3.75	-6.54	0.44	10	0.85	2.01	3.84	2.64	3.47	0.15M NaCl	[39]
Gliclazide	A	5.49		25	0.048	**0.036**	0.034	1	14	3	0.74	2.2	1.51	-4.35	0.32	5	0.59	1.66	2.54	1.93	2.28		[39]
Gliclazide	A	5.49		25	0.048	**0.049**	0.042	1	18	4	0.76	3.1	1.51	-4.35	0.32	5	0.59	1.66	2.54	1.93	2.28	0.15M NaCl	[39]
Glimepiride	A	5.62		25	0.004	**0.010**	0.010	1	7.4	1	0.65	0.6	2.94	-7.09	0.57	6	0.75	2.15	3.50	2.41	3.63		[39]
Glimepiride	A	5.62		25	0.004	**0.020**	0.020	1	14	2	0.63	1.3	2.94	-7.09	0.57	6	0.75	2.15	3.50	2.41	3.63	0.15M NaCl	[39]
Glipizide	A	5.13		25	0.016	**0.011**	0.010	1	5.8	1	0.66	0.7	2.01	-5.53	0.17	6	0.85	2.19	3.71	2.52	3.21		[39]

Table 1. Continued…

Compound	Type	pK_a (acid)	pK_a (base)	t(`C)	k (calc) [b]	k (obs) [c]	± SD	N [d]	log K_n [e]	n	f_{bm}	N_d	log P_{oct}	log S_0	±SD	N	$\Sigma\alpha_2^H$	$\Sigma\beta_2^H$	π_2	R_2	V_x	Comments	Ref
Glipizide	A	5.13		25	0.016	**0.011**	0.010	1	5.8	1	0.67	0.7	2.01	-5.53	0.17	6	0.85	2.19	3.71	2.52	3.21	0.15M NaCl	[39]
Hydrocortisone	N			25	0.219	**0.172**	0.065	7?	35	11	0.97	10.7	1.61	-3.04	0.07	15	0.73	1.90	2.92	2.04	2.80		[40]
Ibuprofen	A	4.25		37	0.100	**0.294**		1	68	19	0.96	18.2	4.13	-3.53	0.20	18	0.57	0.51	1.01	0.78	1.78	0.1M HCl, pH 1.2	[41]
Ibuprofen	A	4.24		25	0.086	**0.248**	0.004	9	61	16	0.96	15.4	4.13	-3.70	0.20	18	0.57	0.51	1.01	0.78	1.78		[42]
Ibuprofen	A	4.24		27	0.086	**0.362**	0.017	5	87	23	0.98	22.4	4.13	-3.70	0.20	18	0.57	0.51	1.01	0.78	1.78		[43]
Ibuprofen	A	4.24		27	0.086	**0.255**	0.013	6	61	16	0.99	15.8	4.13	-3.70	0.20	18	0.57	0.51	1.01	0.78	1.78		[44]
Ibuprofen	A	4.25		37	0.100	**0.409**	0.016	6	93	26	0.98	25.4	4.13	-3.53	0.20	18	0.57	0.51	1.01	0.78	1.78		[44]
Indomethacin	A	4.13		37	0.021	**0.024**	0.000	6	11	2	0.73	1.5	3.51	-5.23	0.22	20	0.57	1.24	2.49	2.44	2.53		[45]
Ketoprofen	A	4.00		37	0.132	**0.840**	0.097	3	173	53	0.98	52.1	3.16	-3.23	0.25	19	0.57	0.87	1.97	1.56	1.98	pH 4.0	[46]
Ketoprofen	A	4.00		37	0.132	**0.946**	0.093	3	193	59	0.99	58.7	3.16	-3.23	0.25	19	0.57	0.87	1.97	1.56	1.98	pH 4.6	[46]
Ketoprofen	A	4.00		37	0.132	**1.052**	0.117	3	215	66	0.99	65.2	3.16	-3.23	0.25	19	0.57	0.87	1.97	1.56	1.98	pH 6.0	[46]
Ketoprofen	A	4.00		37	0.132	**1.091**	0.045	3	222	68	0.99	67.6	3.16	-3.23	0.25	19	0.57	0.87	1.97	1.56	1.98	pH 6.8	[46]
Loratadine	B		5.25	25	0.027	**0.119**		1	42	8	0.92	7.4	5.20	-5.17	0.30	3	0.00	1.14	2.09	2.19	2.87		[47]
Mefenamic Acid	A	4.19		37	0.0089	**0.0036**	0.0002	8	5.6	1	0.22	0.2	5.12	-6.19	0.38	8	0.65	0.70	1.47	1.65	1.92	50 mM PO4	[41]
Mefenamic Acid	A	4.19		37	0.0089	**0.0044**	0.0001	6	5.8	1	0.27	0.3	5.12	-6.19	0.38	8	0.65	0.70	1.47	1.65	1.92	50 mM PO4 + 100 mM NaCl	[41]
Mefenamic Acid	A	4.19		37	0.0089	**0.0036**	0.0003	6	5.6	1	0.22	0.2	5.12	-6.19	0.38	8	0.65	0.70	1.47	1.65	1.92	50 mM PO4 + 50 mM NaCl	[41]
Nimesulide	A	6.31		37	0.046	**0.017**		1	8.8	2	0.52	1.0	2.39	-4.38	0.24	4	0.43	1.10	2.68	2.03	1.99	50 mM PO4, *pH* 6.8	[41]
NSC-639829	B		3.76	25	0.002	**0.058**	0.005	8	30	4	0.90	3.6	6.21	-7.24	0.06	1	0.60	2.03	3.25	3.00	3.12		[48]
Oxazepam	B		1.90	24	0.111	**0.167**	0.003	3	46	11	0.94	10.3	2.24	-4.03	0.17	5	0.64	1.29	1.75	2.23	1.99		[36]
Paraben,Et-	A	8.35		24	0.313	**0.478**	0.017	3	70	30	0.99	29.7	2.47	-2.28	0.07	6	0.66	0.72	1.25	0.87	1.27		[36]
Paraben,Me-	A	8.35		24	0.476	**0.561**	0.037	3	66	35	0.99	34.8	1.96	-1.82	0.11	8	0.66	0.72	1.24	0.87	1.13		[36]
Paraben,Me-	A	8.35		24	0.476	**0.340**	0.010	3	41	22	0.96	21.1	1.96	-1.82	0.11	8	0.66	0.72	1.24	0.87	1.13	0.15M NaCl	[36]
Paraben,n-Bu-	A	8.47		24	0.177	**0.641**	0.001	3	118	40	0.99	39.7	3.57	-2.91	0.15	13	0.66	0.73	1.26	0.87	1.55		[36]
PG-300995	B		3.58	25	0.192	**0.085**	0.006	5	22	6	0.88	5.3	2.60	-3.59	0.03	1	0.35	0.74	1.78	2.12	1.40	pH 1.0	[49]

Table 1. Continued…

Compound	Type	pK_a (acid)	pK_a (base)	t(`C)	k (calc) [b]	k (obs) [c]	± SD	N [d]	log K_n [e]	n	f_{bm}	N_d	log P_{oct}	log S_0	±SD	N	$\Sigma\alpha_2^H$	$\Sigma\beta_2^H$	π_2	R_2	V_x	Comments	Ref
PG-300995	B		3.58	25	0.192	**0.082**	0.003	9	7	6	0.00	5.1	2.60	-3.59	0.03	1	0.35	0.74	1.78	2.12	1.40	pH 2.0	[49]
PG-300995	B		3.58	25	0.192	**0.081**	0.004	5	19	6	0.00	5.0	2.60	-3.59	0.03	1	0.35	0.74	1.78	2.12	1.40	pH 3.0	[49]
PG-300995	B		3.58	25	0.192	**0.022**	0.001	5	7.5	2	0.68	1.4	2.60	-3.59	0.03	1	0.35	0.74	1.78	2.12	1.40	pH 7.0	[49]
Phenytoin	A	8.28		25	0.063	**0.023**	0.0002	4	8.5	2	0.73	1.5	2.24	-4.05	0.11	21	0.44	1.14	2.04	1.94	1.87		[50]
Pioglitazone	AB	5.63	6.63	25	0.028	**0.023**	0.023	1	13	2	0.72	1.4	2.94	-6.32	0.23	2	0.34	1.64	2.37	2.33	2.66		[39]
Pioglitazone	AB	5.63	6.63	25	0.028	**0.026**	0.025	1	13	2	0.80	1.6	2.94	-6.32	0.23	2	0.34	1.64	2.37	2.33	2.66	0.15M NaCl	[39]
Piroxicam	AB	1.76	4.96	37	0.023	**0.019**	0.001	3	8.8	2	0.58	1.2	1.98	-4.33	0.33	18	0.72	2.12	3.12	2.56	2.16	pH 4.0	[51]
Piroxicam	AB	1.76	4.96	37	0.023	**0.020**	0.002	3	8.8	2	0.60	1.2	1.98	-4.33	0.33	18	0.72	2.12	3.12	2.56	2.16	pH 5.0	[51]
Piroxicam	AB	1.76	4.96	37	0.023	**0.018**	0.002	3	8.8	2	0.55	1.1	1.98	-4.33	0.33	18	0.72	2.12	3.12	2.56	2.16	pH 6.0	[51]
Piroxicam	AB	1.76	4.96	37	0.023	**0.031**	0.0004	3	10	2	0.96	1.9	1.98	-4.33	0.33	18	0.72	2.12	3.12	2.56	2.16	pH 7.0	[51]
Piroxicam	AB	1.76	4.96	37	0.023	**0.018**	0.044	3	8.8	2	0.56	1.1	1.98	-4.33	0.33	18	0.72	2.12	3.12	2.56	2.16	pH 7.8	[51]
Prazepam	B		3.04	24	0.199	**0.154**	0.005	3	37	10	0.96	9.6	3.73	-3.56	0.23	2	0.00	1.05	1.81	2.32	2.39		[36]
Progesterone	N			25	0.139	**0.126**	0.166	7?	38	8	0.98	7.8	3.77	-4.53	0.22	12	0.00	1.04	2.49	1.56	2.62		[40]
Progesterone	N			24	0.139	**0.227**	0.006	3	69	15	0.94	14.1	3.77	-4.53	0.22	12	0.00	1.04	2.49	1.56	2.62		[36]
Progesterone	N			24	0.139	**0.150**	0.001	3	46	10	0.93	9.3	3.77	-4.53	0.22	12	0.00	1.04	2.49	1.56	2.62	0.15M NaCl	[36]
Progesterone,11-α-HO-	N			24	0.122	**0.276**	0.007	3	82	18	0.95	17.1	2.36	-4.51	0.39	5	0.31	1.35	2.75	1.77	2.68		[36]
Repaglinide	AB	3.83	6.20	25	0.034	**0.038**	0.037	1	15	3	0.79	2.4	4.69	-4.89	0.16	2	0.83	1.71	2.77	2.17	3.68		[39]
Repaglinide	AB	3.83	6.20	25	0.034	**0.045**	0.044	1	16	3	0.93	2.8	4.69	-4.89	0.16	2	0.83	1.71	2.77	2.17	3.68	0.15M NaCl	[39]
Resveratrol	A	9.8 8.8		25	0.097	**0.032**	0.002	4	9.2	2	0.99	2.0	3.14	-3.57	0.18	7	1.50	1.04	1.82	1.97	1.74	pH 8.0	[52]
Resveratrol	A	9.8 8.8		25	0.097	**0.023**	0.001	4	7.5	2	0.71	1.4	3.14	-3.57	0.18	7	1.50	1.04	1.82	1.97	1.74	pH 8.0, 0.3M NaCl	[52]
Resveratrol	A	9.8 8.8		25	0.097	**0.033**	0.001	4	11	3	0.68	2.1	3.14	-3.57	0.18	7	1.50	1.04	1.82	1.97	1.74	pH 8.0, 2M urea	[52]
Rosiglitazone	AB	6.23	6.51	25	0.027	**0.027**	0.025	1	11	2	0.83	1.7	2.56	-5.05	0.24	2	0.34	1.88	2.64	2.55	2.61		[39]

Table 1. Continued…

Compound	Type	pK_a (acid)	pK_a (base)	t(`C)	k (calc) [b]	k (obs) [c]	± SD	N [d]	log K_n [e]	n	f_{bm}	N_d	log P_{oct}	log S_0	±SD	N	$\Sigma\alpha_2^H$	$\Sigma\beta_2^H$	π_2	R_2	V_x	Comments	Ref
Rosiglitazone	AB	6.23	6.51	25	0.027	**0.032**	0.030	1	12	2	1.00	2.0	2.56	-5.05	0.24	2	0.34	1.88	2.64	2.55	2.61	0.15M NaCl	[39]
Salicylic Acid	A	2.84		27	0.467	**0.544**	0.066	6	65	34	0.99	33.7	2.19	-1.84	0.07	12	0.70	0.40	1.10	0.91	0.99		[44]
Temazepam	B		1.60	24	0.366	**0.416**	0.014	3	82	26	0.99	25.8	2.19	-3.07	0.54	2	0.17	1.34	1.76	2.24	2.13		[36]
Testosterone	N			24	0.181	**0.208**	0.004	3	55	13	0.99	12.9	3.31	-4.09	0.07	13	0.31	1.01	2.27	1.55	2.38		[36]
Testosterone	N			25	0.181	**0.115**	0.060	7?	34	8	0.89	7.1	3.31	-4.09	0.07	13	0.31	1.01	2.27	1.55	2.38		[40]
Toluic Acid,3-	A	4.26		35	0.865	**1.199**	0.009	6	124	75	0.99	74.3	2.39	-1.63	0.38	3	0.57	0.44	1.02	0.77	1.07		[31]
Toluic Acid,4-	A	4.35		35	0.545	**0.375**	0.006	6	52	24	0.97	23.2	2.29	-2.11	0.51	5	0.57	0.44	1.02	0.77	1.07		[31]
Valsartan	A	4.70 3.60		25	0.087	**0.313**	0.005	8	75	20	0.97	19.4	3.90	-3.69	0.36	4	1.21	1.82	3.32	2.96	3.41		[53]

[a] K_n = drug-micelle binding constant, where n drugs are bound to one micelle; N_d = average number of bound drugs per micelle; f_{bm} = fraction of drug-bound micelles; P_{oct} = octanol-water partition coefficient; S_0 = intrinsic solubility, average of N published values; $\Sigma\alpha_2^H$, ... , V_x are the calculated Abraham solvation descriptors (cf., Glossary).

[b] Calculated from expressions in Table 2.

[e] Calculated using Eq. (13).

With water solubility determined from the horizontal portions of the curves (or taken from literature sources), and with the k values determined from the micellar portions of the plots, it was possible to approximate the drug-micelle binding constants, log K_n, according to Eq. (13). The stoichiometric coefficient, n, was selected according to Eq. (14). These estimated results are listed in Table 1.

Prediction Model for k Values

In a comprehensive study, Abraham *et al.* [58] considered the SDS-water partitioning of a large number of molecules (*e.g*., gases, common solvents, polycyclic aromatics, carboxylic acid and phenol derivatives, *etc.*) and developed tight prediction equations based on octanol-water partition coefficients, as well as the five Abraham solvation descriptors (r^2 = 0.97, SD = 0.17 log unit, F = 817, N = 132). The micelles were treated as a separate phase in the two-phase (aqueous-micellar) media. The SDS-water partition coefficients, $P_{SDS\text{-}water}$, can be converted into k values, as mentioned above [12]. Apparently, the prediction study had not been extended to drug molecules which precipitate in SDS-containing solutions to form three-pseudophase systems (aqueous, solid, micellar). By contrast, attention in the present study was directed mainly towards poorly-soluble drug molecules (Table 1). As the discussion has stressed, a drug-micelle *binding* paradigm (*i.e*., mass action model) is used here, rather than a partitioning approach chosen by Abraham *et al.* [58].

Several comparisons were made in an attempt to find predictive correlations between k and other commonly-available physicochemical descriptors. Figure 8a shows the plot of measured log k values as a function of octanol-water partition coefficients, log P_{oct}. The trend suggests that solubilization capacity of drugs decreases as lipophilicity increases, but the correlation is clearly weak. A similar trend, albeit with only slightly improved correlation, is noted when log k is plotted against size of molecules in Figure 8b. For smaller sets of homologous compounds, better correlations have been observed. For example, Fahelelbom *et al.* [30] reported r^2 = 0.85 for the correlation between k and molar volume for six iminophenazine derivatives (*cf*., six squares for log k < -3 in Fig. 8b).

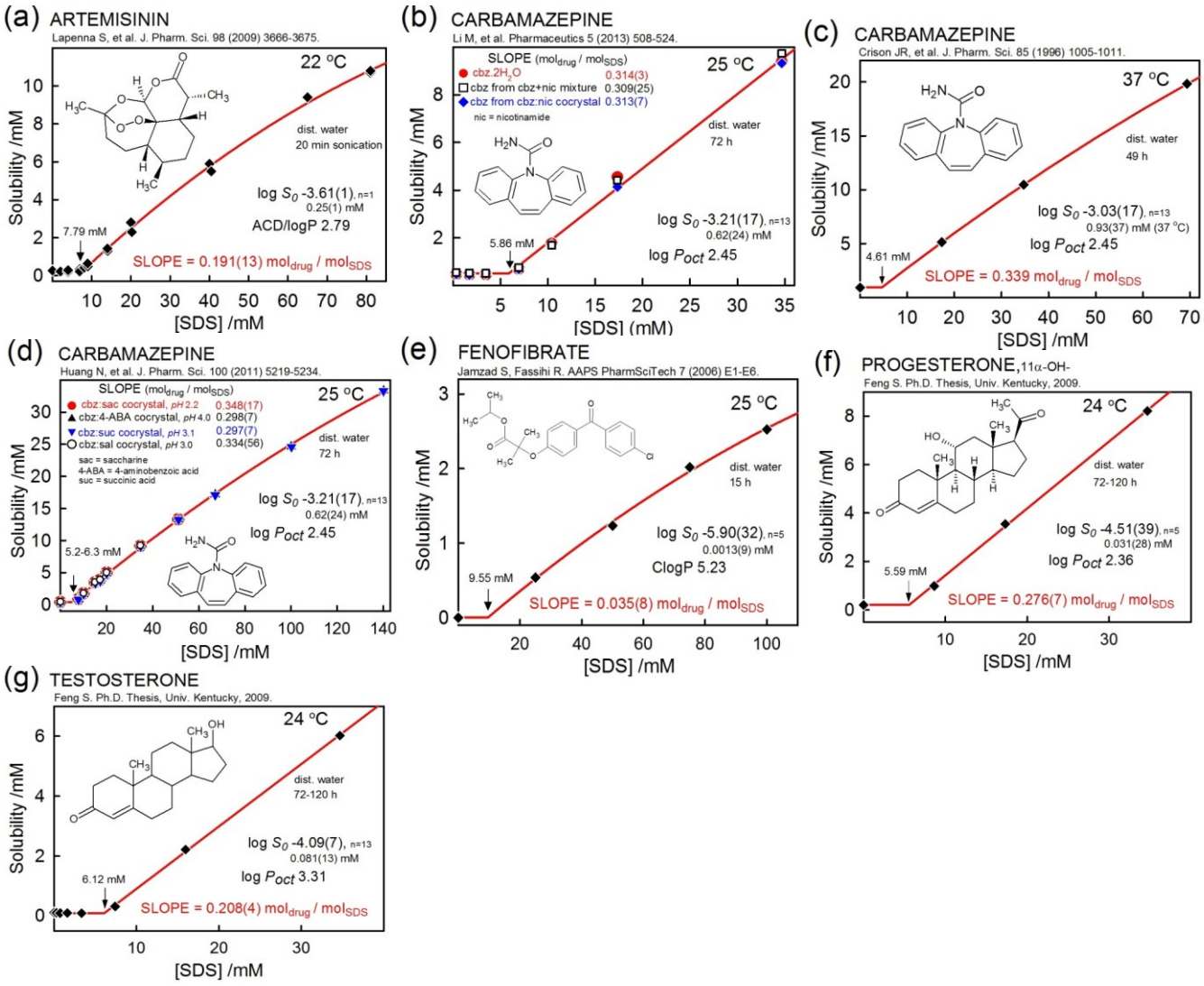

Figure 2. Examples of micellization plots of *nonionizable* drugs. The CMC values span from 4.6 to 9.6 mM, which suggests that the drugs had only a small influence on the onset of micelle formation with increasing SDS additions to distilled water. The [SDS] > CMC curves show slight curvature for artemisinin, carbamazepine, and fenofibrate. These are the cases of [SDS] exceeding 40 mM, which may suggest a saturation/decrease of the capacity to bind these uncharged drugs. The n values in Table 1 indicate that 19-22 carbamazepine molecules bind to a single micelle above the CMC. The n values for artemisinin, 11α-hydroxyprogesterone, and testosterone are estimated to be 12, 18, and 13, respectively. Just 3 fenofibrate bind to one SDS micelle, given that the drug is so poorly soluble (0.0013 mM). The solubility of the other drugs ranges from 0.03 to 0.93 mM. The drug-micelle binding constants, K_n (*cf.*, Eq. (13)), range from 10^{+18} (fenofibrate) to 10^{+82} M^{-n} (11α-hydroxyprogesterone). Pure carbamazepine or carbamazepine released from cocrystals appears to indicate the same micellization slopes. Also, the slopes at 25 and 37 °C appear to be nearly the same for the drug.

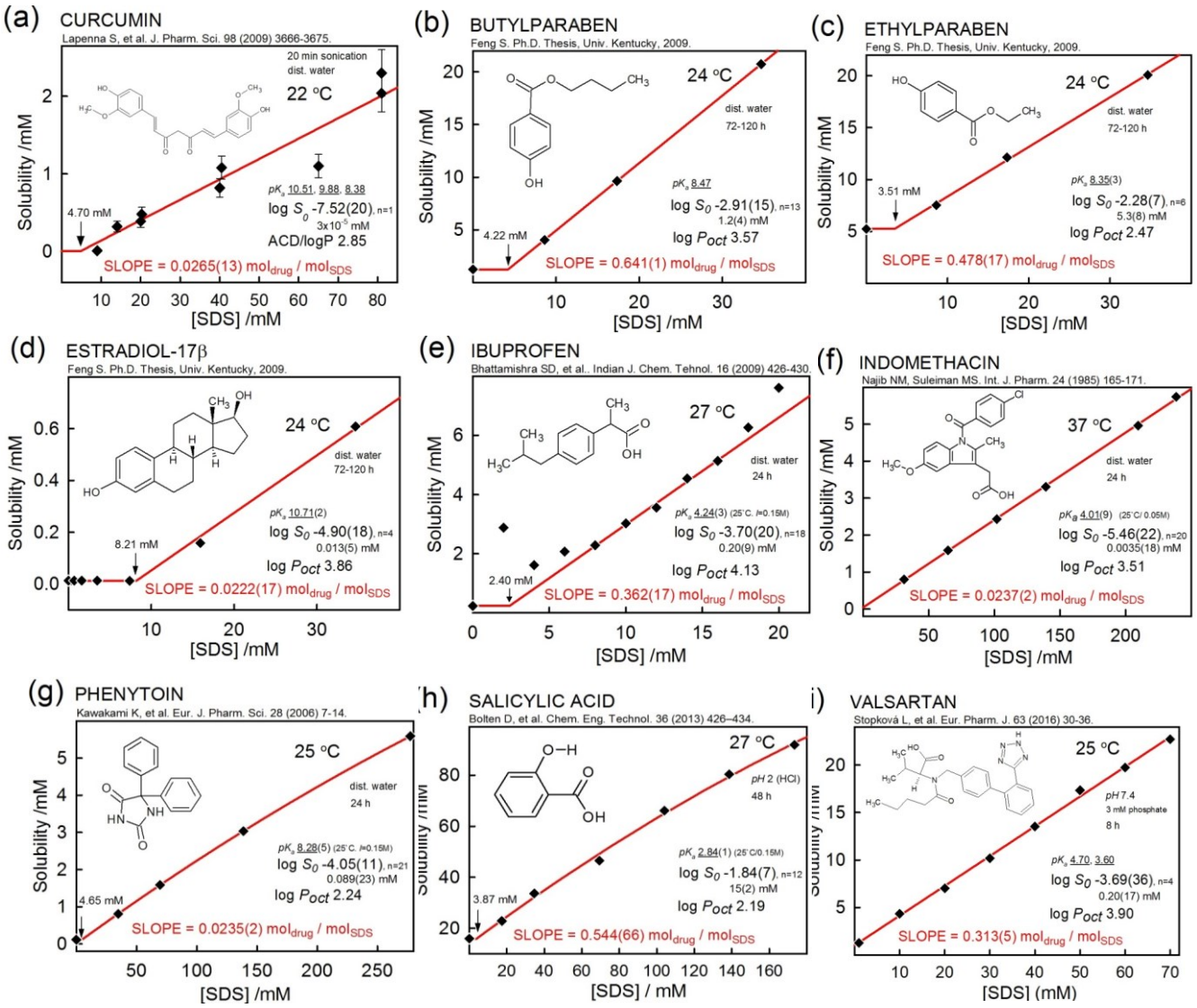

Figure 3. Examples of micellization plots of largely nonionized *acidic* drugs. In the first seven frames, the medium was distilled water. In Figure 3h, HCl was added to adjust the solution to pH 2 (where salicylic acid is largely uncharged). In Figure 3i, 3 mM phosphate buffer at pH 7.4 was used, although *p*DISOL-X calculation suggests that in the low buffer capacity solution, the pH may have been as low as 4.2 (the final pH values of the valsartan solutions were not reported). In these cases, it was assumed that ionization of the acids was insignificant. Most of the CMC values are in the interval 2.4-8.2 mM. The micellar-portion curves show slight curvature for phenytoin (g) and salicylic acid (h), as the surfactant concentrations extend to 277 and 173 mM, respectively. Indomethacin (f) also extends to high surfactant concentrations (238 mM) but does not indicate nonlinearity. In the plots of indomethacin and valsartan, the CMC is very close to zero. The data in the case of ibuprofen (e) show peculiar variance, for [SDS] < 7 and > 15 mM. Four of the low-soluble compounds bind as 2 drugs per micelle, with K_n ranging from $10^{+8.5}$ (phenytoin) to 10^{+16} (curcumin). Values of n for the more soluble drugs range from 20 (valsartan) to 40 (butylparaben), with corresponding K_n values from 10^{+75} to 10^{+118} M^{-n}, respectively (*cf.*, Table 1).

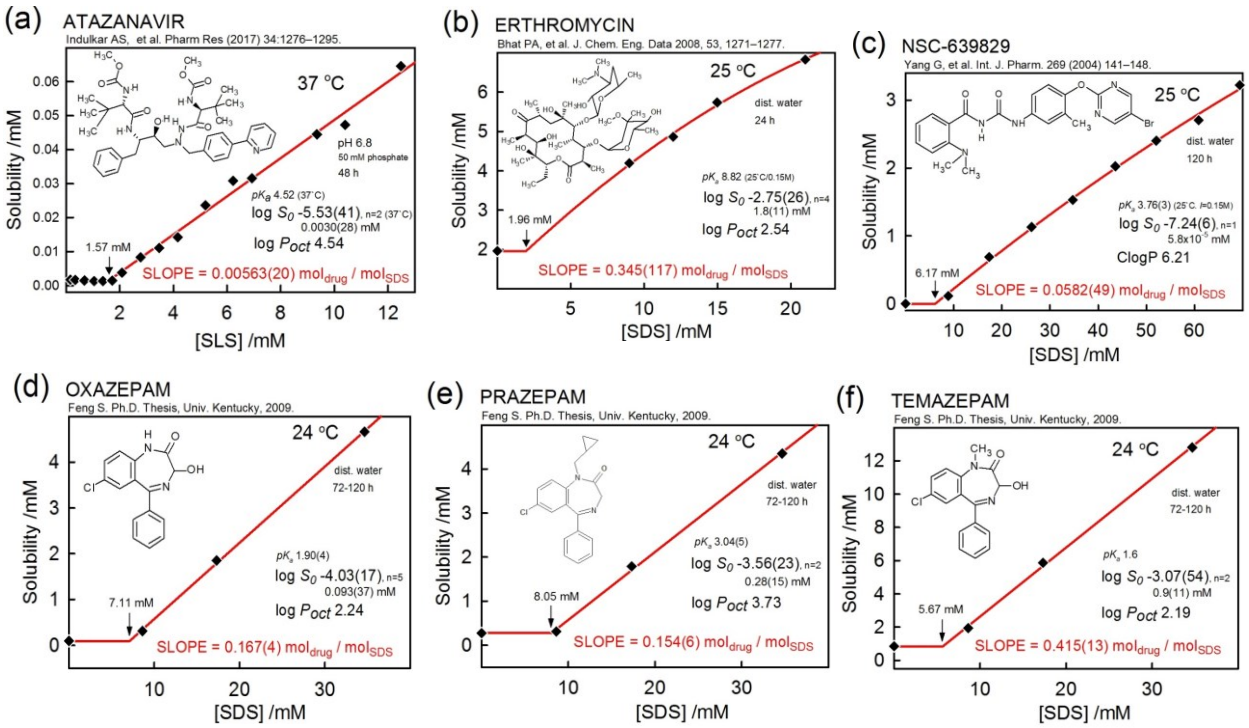

Figure 4. Examples of micellization plots of largely nonionized *basic* drugs. Erythromycin (b) and NSC-639829 (c) show curvature in the micellar portion of the curves, even over relatively low surfactant concentrations. Atazanavir binds 1:1 with micelles, with $K_1 = 10^{+5.3}$ M^{-1}(Eq. 13). The most insoluble of the bases, NSC-639829, binds as 4:1 with micelles, with $K_4 = 10^{+30}$ M^{-4}. The other values of n range from 10 to 26 (*cf.*, Table 1).

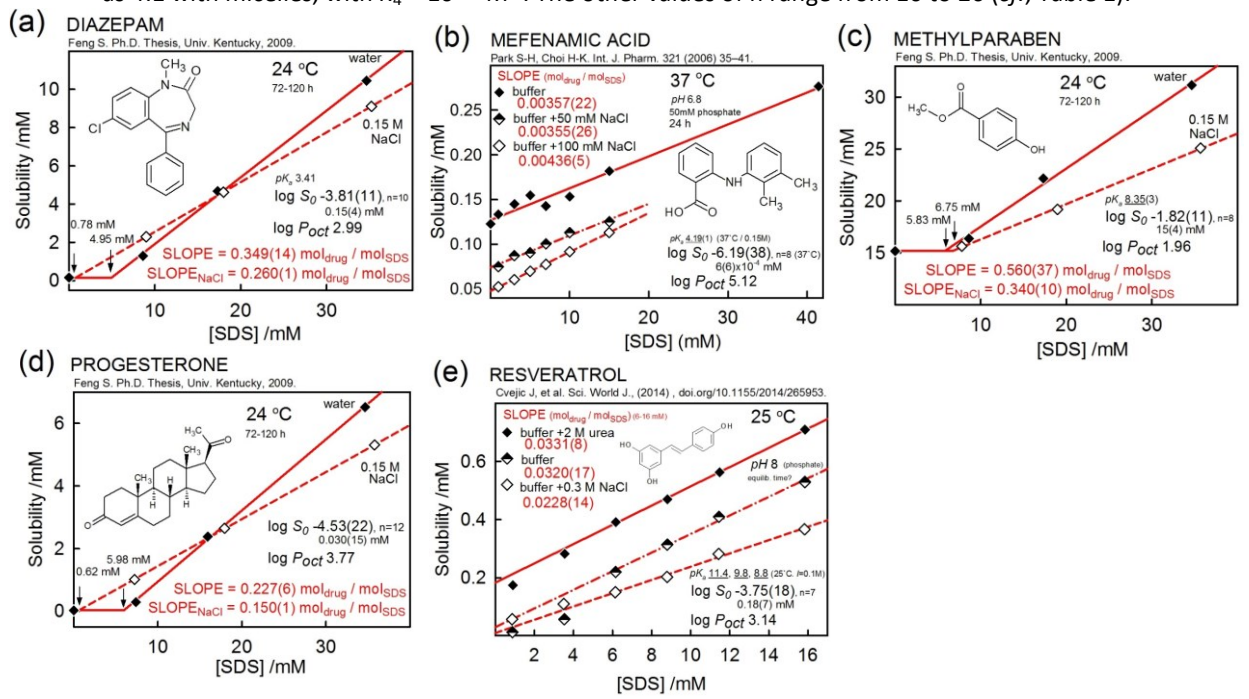

Figure 5. Examples of the *effect of salt* on micellization. With the apparent exception of buffered solutions of mefenamic acid (S_0 = 0.6 µM) and, to a lesser extent, of resveratrol (S_0 = 180 µM), the examples comparing water to 0.15 M NaCl solutions show that κ values decrease with increasing salt. Also, the CMC decreases with increasing salt concentration, an effect expected from properties of SDS in the absence of drug, as illustrated in Figure 1. With lower CMC, the micelle structures become more stabilized due to reduced head group charge repulsions, which lead to reduced drug solubilization. The addition of buffer, as in the cases of mefenamic acid (b) and resveratrol (e) contributes to the ionization of the drugs, which impacts on the solubility, but not so much on the solubilization capacity.

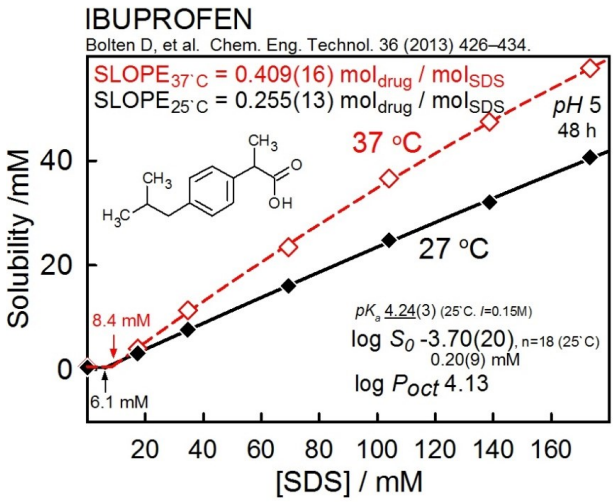

Figure 6. Example of the effect of *temperature* on micellization. Ibuprofen shows higher degree of solubilization at 37 °C (26 drugs/micelle, Table 1), compared to 27 °C (16 drugs/micelle). The CMC is only slightly elevated at the higher temperature. The formation of micelles is entropy driven, due to the release of water structure surrounding hydrophobic groups, as these groups migrate into the micelle core [12]. Above 60 °C, water loses most of its ability to form cavities around hydrophobic groups, so the drive to form micelles is weakened at elevated temperature, indicated by increased CMC [11, 12]. Urea also plays a role in "water structure breaking."

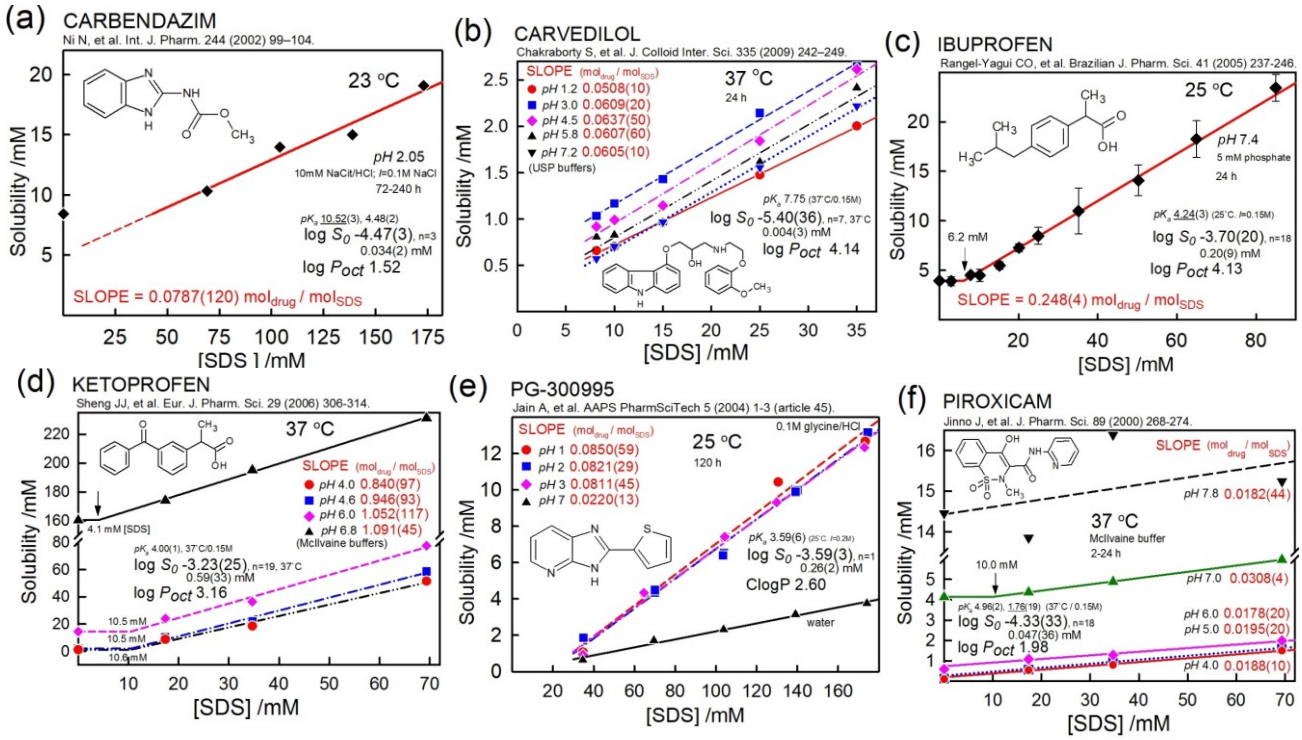

Figure 7. Examples of effect of pH on micellization. When pH of the medium is adjusted with buffers, the calculated water solubility needs to take into account the pK_a of the molecule. Sub-CMC data for carvedilol (b) and PG-300995 (e) are not shown, as these involve the precipitation of the cationic drugs and the anionic surfactant. With the added complexity, these molecules are further discussed in a separate section below. With the exception of PG-300995 (e), the k values do not show appreciable dependence on pH, as indicated in frames (b), (d), and (f). The mass action equilibrium model can rationalize the k-pH dependence of PG-300995 (below).

A significantly improved correlation (r^2 = 0.69) is evident between measured log k and log S_0, as shown in Figure 8c. This might have been anticipated by Eq. (13). The standard deviation, SD = 0.50 log unit, is suggestive of the 0.6-0.7 log unit often cited interlaboratory reproducibility in drug solubility measurement, although reproducibility could be improved if the solubility data were critically processed [55]. An examination of Figure 8c suggests that acids (red circles) tend to distribute below the correlation line for S_0 > 1 μM, suggesting that acid-base properties might correlate with k values.

To test the k data for further relationships, the 101-molecule set was subdivided into four groups, differentiated by acid-base indicator indices (0/1), I_A, I_B, I_{AB}, I_N, to designate each drug as an acid, base, ampholyte, or neutral type, respectively (Table 1). Each k sub-group of drugs was tested separately, using log S_0, and just one of each of the five Abraham [59] solvation descriptors ($\Sigma\alpha_2^H$, $\Sigma\beta_2^H$: H-bond acidity and basicity; π_2: dipolarity/polarizability; R_2: dispersion force; and V_x: molar volume – see Glossary for further elaboration; Table 1 lists the five descriptors). The five descriptors were estimated from the 2D structure of molecules. Table 2 lists the results of the best-fitting combination of descriptors (no more than two per acid-base sub-group). Inclusion of Abraham H-bond descriptors only slightly improved the fitting (r^2 increased from 0.69 to 0.74). Generally, the distribution of solute between the water, solid, and micelles is tilted towards the solid state for highly insoluble drugs, as evidenced by decreased solubilization capacity. In the case of acids, strong H-bond donor character leads to decreased solubilization capacity; for non-ionizable drugs and for ampholytes, strong H-bond acceptor character leads to decreased solubilization by SDS. In the case of ampholytes, most of the variance is accounted by $\Sigma\beta_2^H$, while log S_0 appears to be of minimal importance (Table 2).

Figure 8d shows the final best-fit model correlation plot (although it is hardly better than that in Fig. 8c). The four acid-base group analyses were combined into a single multiple linear regression (MLR) equation:

$$\log k = \{ c_0 + c_1 \cdot \log S_0 + c_2 \cdot \Sigma\alpha_2^H \} \cdot I_A + \{ c_3 + c_4 \cdot \log S_0 \} \cdot I_B + \{ c_5 + c_6 \cdot \log S_0 + c_7 \cdot \Sigma\beta_2^H \} \cdot I_N + \{ c_8 + c_9 \cdot \log S_0 + c_{10} \cdot \Sigma\beta_2^H \} \cdot I_Z \quad (15)$$

Table 2. Prediction of k values [a]

Class	Equation	r^2	SD	F	N
Nonionizables	log k = 0.479 + 0.249 log S_0 -0.201 $\Sigma\beta_2^H$	0.70	0.15	17	17
Acids	log k = 1.011 + 0.417 log S_0 -0.692 $\Sigma\alpha_2^H$	0.71	0.49	54	47
Bases	log k = 1.228 + 0.542 log S_0	0.74	0.57	66	25
Ampholytes	log k = -0.122 + 0.083 log S_0 -0.548 $\Sigma\beta_2^H$	0.79	0.10	17	12
Overall based on Eq. (15)		0.74	0.44	288	101

[a] Σα2H and Σβ2H are the calculated Abraham H-bond total acidity and basicity descriptors, resp.;
r^2 = squared multiple correlation coefficient; SD = standard deviation in the linear fit;
F = measure of predictive capability: how much of the variance is explained by the model per parameter; N = number of k values used.

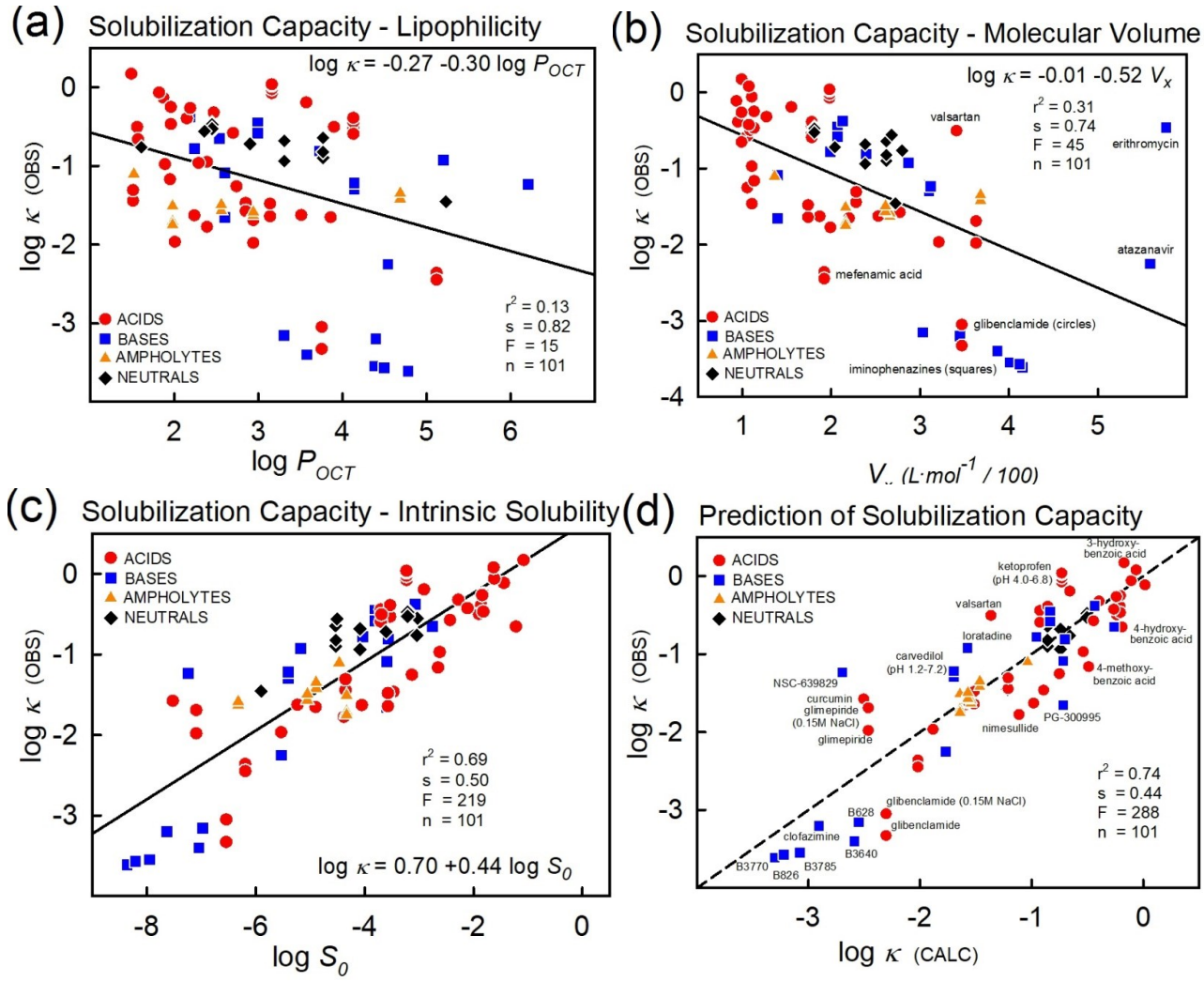

Figure 8. Correlations between log k and (a) octanol-water partition coefficients, log P_{oct}, (b) McGowan molecular volume, V_x, in units of 0.01 L·mol^{-1} (c) intrinsic solubility, log S_0 (molarity), and (d) multiple linear regression with data grouped according to acid-base classes, using log S_0, $\Sigma\alpha_2^H$, and $\Sigma\beta_2^H$ as descriptors (*cf.*, Table 2).

The best-fit MLR coefficients, c_0-c_{10} are listed in Table 2. The combined set yielded r^2 = 0.74, SD = 0.44, F = 288, N = 101. The compounds with the lowest intrinsic solubility (*e.g.*, NSC-639829, curcumin, glibenclamide) showed the highest variances, as indicated in Figure 8d. The erythromycin outlier may be due to unaccounted precipitation of the drug-SDS salt [61]. In sum, it appears that the combined quality of the experimental k and S_0 data limited further improvements of the prediction model.

In-Depth Treatment of pH Dependence of k Values

The data below the CMC for carvedilol (Fig. 7b) and PG-300995 (Fig. 7e) take on a complex dependence on pH and SDS concentration, and will be examined here in detail. As the SDS decreases below the CMC, the solubility of the two molecules actually *increases*, in contrast to all the preceding examples (Figs. 2-6). This can be explained by the precipitation of salt formed between positively charged drug and the SDS anions, and confirmed by speciation regression analysis. The same may be taking place for carbendazim at pH 2.05 in

Figure 7a, but there was not enough data reported to test this. However, there were sufficient pre-CMC measurements in the cases of carvedilol and PG-300995, particularly in the latter case.

Carvedilol

Chakraborty *et al*. [35] studied the micellization of carvedilol at 37 °C in the pH 1.2-7.2 range, where the drug was largely positively charged. The authors suggested that anionic SDS interacted with the cationic drug species to form an insoluble drug salt. The k values (Fig. 7b) did not change across the pH range considered, which is expected if only the neutral form of the drug were solubilized by SDS micelles. There were not a lot of data in the pre-CMC region, but it was possible to estimate log $K_{sp}^{BH.Cl}$ = -3.88 (from surfactant-free solubility data) and log $K_{sp}^{BH.SDS}$ = -5.52 (from data at $[SDS]_{tot}$ = 5 mM).

PG-300995

There were ample data, both pre- and post-CMC, for the case of PG-300995 (2-(2-Thienyl)-1H-imidazo[4,5-b]pyridine) reported by Jain *et al.* [49] to allow for further analyses here. The solubility-pH data at 25 °C, I = 0.2M, in SDS-free, buffered solutions [60] were re-analyzed using *p*DISOL-X, to obtain pK_a = 3.59 ± 0.06, log S_0 = -3.59 ± 0.03, and log $K_{sp}^{BH.Cl}$ = -2.12 ± 0.11, GOF = 0.84, n = 11. Jain *et al.*[49] had proposed that the positively-charged drug precipitates as the (estolate) salt with anionic SDS in the pre-CMC region. Erythromycin is another rare example of such an estolate salt formation [61]. However, the solubilization of the salt is not evident in Figure 4b. It is estimated that the solution pH is 9.7 (not reported by Bhat *et al.* [37]).

The PG-300995 data across the whole range of SDS concentrations were analyzed by the mass action model, employing one heterogeneous and three homogeneous equilibrium equations. The drug is uncharged at pH 7, and the micellization behavior is relatively simple. Figure 9a shows the drug solubility as a function $[SDS]_{tot}$. The red curve was calculated using the mechanistic model described by Eqs. (2)-(4), with n = 2. (This is nearly, but not precisely, the same as the empirical fit of the pH 7 curve in Figure 7e.) The best-fit constants are summarized in the box in Figure 9c. Figure 9b shows the underlying reactant concentrations. These concentrations largely follow the pattern shown in Figure 1a. The solubilization of uncharged drug lowers the CMC to 3.2 mM. This relatively simple pattern of concentrations is expected to be repeated in the examples in Figures 2-6, where the drug in solution is predominantly in the uncharged state. However, the data patterns for PG-300995 at pH 1-3 are quite different, where the drug in solution is predominantly positively charged.

One of the independent variables in the mass action calculations is the actual weight of the API added to solution. Provided enough solid is added to maintain a saturated solution, knowledge of the exact weight is not critical for simple solubilization reactions in drug-saturated solutions under conditions where the drug is uncharged (*i.e.,* at pH 7). Most publications simply state that "excess solid" was added in the solubility assay. The PG-300995 publication falls into this category. However, at pH 1-3, the PG-300995 reactions are not simple. When the cationic drug, BH^+, forms a salt precipitate with SDS^-, then it is necessary to provide the exact analytical weight of the API for the calculation.

Figure 10a shows the drug solubility at pH 1 as a function $[SDS]_{tot}$. Three different $[PG]_{tot}$ were tested in the mass action calculations: 15, 30, and 38 mM (solid, dot, dash curves, resp.). Above the CMC (estimated at 17 mM), it is not critical to the calculation that the actual $[PG]_{tot}$ be provided. "Excess" is sufficient. There, the linear increase in solubility with increasing SDS is compatible with four *protonated* drugs bound per micelle

aggregate. Eq. (13) cannot be used, as noted earlier. The red dashed (38 mM) best-fit curve matches the data at the two lowest and the four highest $[SDS]_{tot}$ points (squares), but not the three points in the middle. The refinement of equilibrium constants (at 38 mM) was carried out by assigning zero weights to the latter three points. The red solid (15 mM) curve is the best fit to all the data, except that of the first two points.

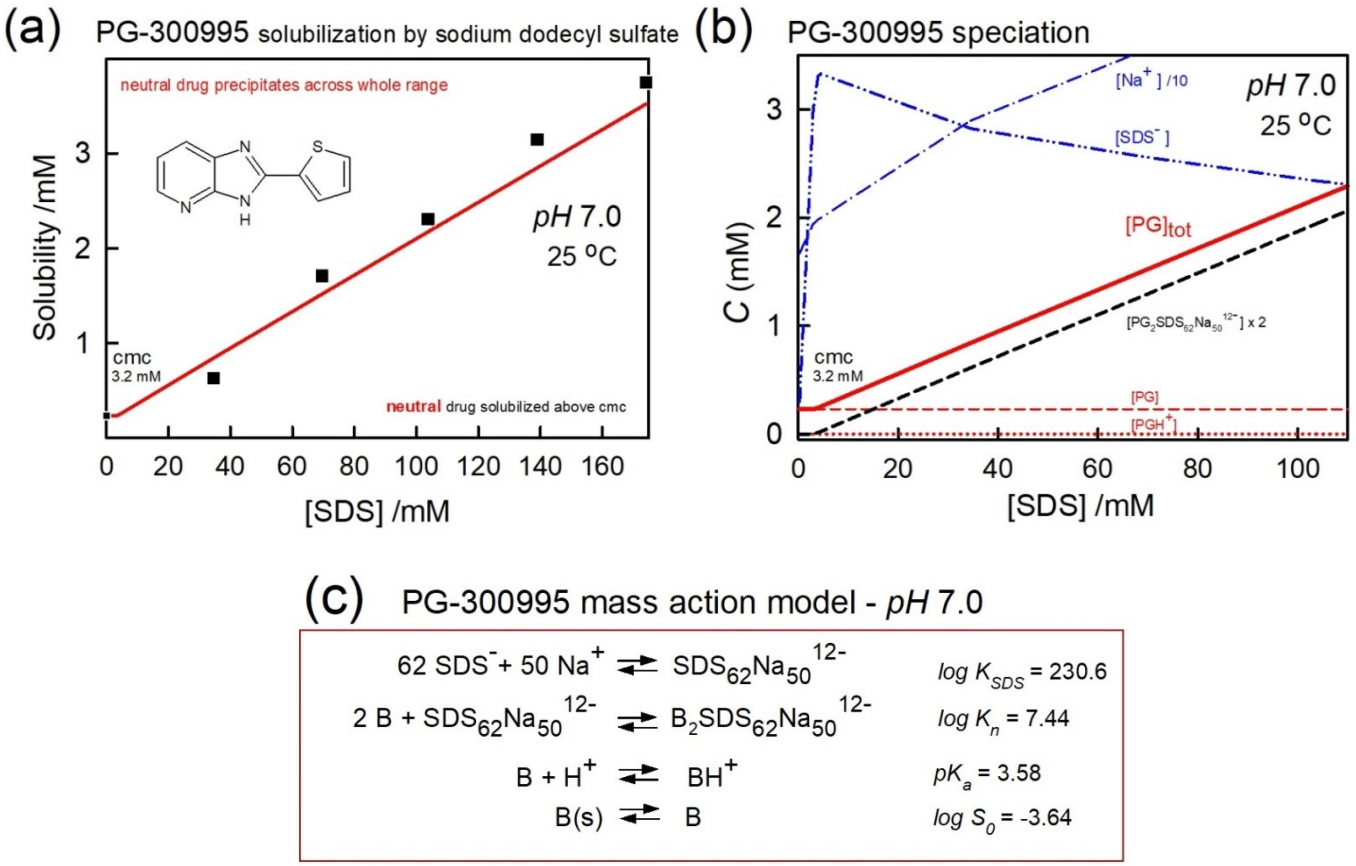

Figure 9. Mass action analysis of the solubilization of PG-300995 at pH 7, where the drug is uncharged. (a) Total drug solubility vs. $\{SDS\}_{tot}$, (b) speciation profile, (c) mass action model summary (B = PG-300995).

The mass action model consisted of three homogeneous and three heterogeneous equilibria, summarized in the box in Figure 10c. For the entire range of SDS values, the precipitated form of the drug is the estolate salt. The hydrochloride salt was included in the analysis, but the data did not support its role in this complicated solubilization system. Figure 10b displays the underlying reactant and complex species formed with increasing SDS for 15 mM total added drug. The curves for some of the species were scaled in order to appear in the same view. The CMC break in the curves occurs at 17 mM, corresponding to an unusually elevated value, suggesting a weakened micellar structure compared to drug-free conditions.

Stabilizing Cocrystal Suspension with SDS

Carbamazepine:Saccharin 1:1 Cocrystal – Experimental Data from Cao et al. [9]

There are very few published examples [9, 33] of eutectic data for both the API and the coformer in assays where surfactant had been added. Cao *et al.* [9] published an in-depth mechanistic dissolution study of the carbamazepine:saccharin 1:1 cocrystal system, which included such eutectic data for both carbamazepine and

saccharin at pH 1 in the presence of 22, 44, 250, and 400 mM SDS. The CC system had been thoroughly studied in surfactant-free media [62-64], and had been subjected to *p*DISOL-X analysis [16, 17].

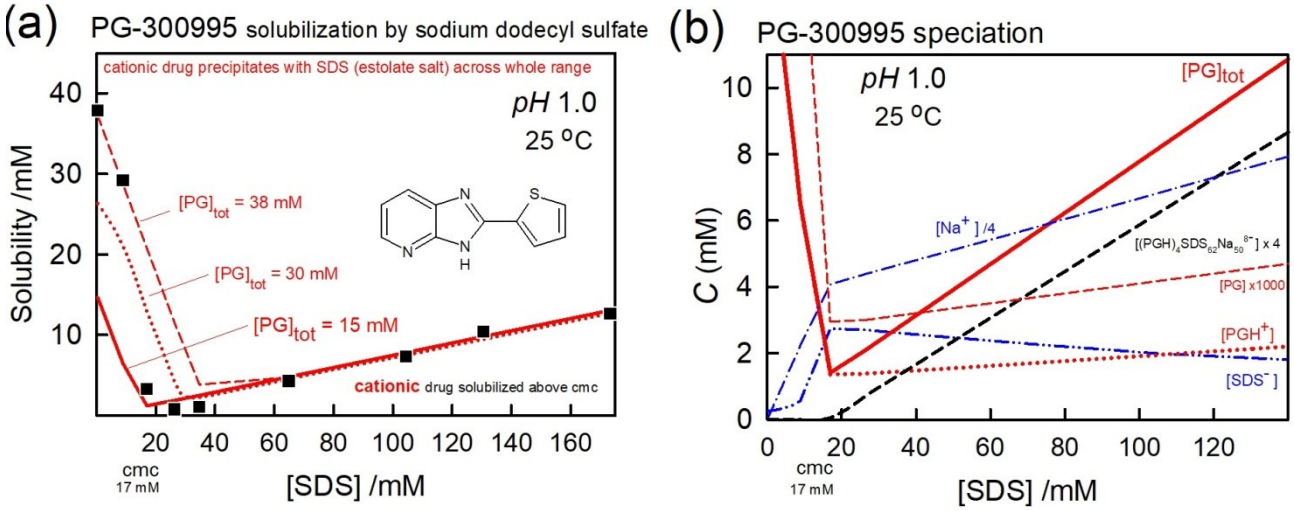

(c) PG-300995 mass action model - *pH* 1.0

$62\ SDS^- + 50\ Na^+ \rightleftharpoons SDS_{62}Na_{50}^{12-}$	$\log K_{SDS} = 230.6$
$4\ BH^+ + SDS_{62}Na_{50}^{12-} \rightleftharpoons (BH)_4SDS_{62}Na_{50}^{8-}$	$\log K_n = 22.97$
$B + H^+ \rightleftharpoons BH^+$	$pK_a = 3.58$
$B(s) \rightleftharpoons B$	$\log S_0 = -3.64$
$BH.SDS(s) \rightleftharpoons BH^+ + SDS^-$	$\log K_{sp}^{BH.SDS} = -5.41$
$BH.Cl(s) \rightleftharpoons BH^+ + Cl^-$	$\log K_{sp}^{BH.Cl} = -2.12$

Figure 10. Mass action analysis of the solubilization of PG-300995 at pH 1, where the drug is positively charged. (a) Total drug solubility vs. $[SDS]_{tot}$ at three levels of total drug concentration, (b) speciation profile at 15 mM total drug concentration, (c) mass action model summary (B = PG-300995).

The non-CC carbamazepine solubility-SDS data at 25 °C [6] in Figure 2d were subjected to mass action analysis to determine the best-fit drug-micelle binding constant, and to attempt to predict the curvature in the post-CMC plots. It was assumed that 22 carbamazepine molecules bind to one SDS micelle aggregate (*cf.*, Table 1). At least three constants were needed to explain the data pattern in Figure 2d: log K_{SDS} = 230.6, log K_{22} = 74.0, log S_0 = -3.33, GOF = 0.50, N = 37. There was a tiny bend in the calculated mass action post-CMC curve (due to ionic strength effects), but not fully matching the extent of the curvature observed for $[SDS]_{tot}$ > 70 mM, where solubilization capacity notably decreased. This was expected to complicate the quantitative assessment of the eutectic data of Cao *et al*. [9], who considered $[SDS]_{tot}$ as high as 400 mM.

From the non-SDS carbamazepine:saccharin 1:1 CC solubility-pH data, the mean of the equilibrium constants reported previously [17, 63, 64] are pK_a^{cof} = 1.31, log K_{sp} = -6.01 and log S_0 = -3.26. One additional constant was needed, K_n^{cof}, before the Cao *et al.* eutectic solubility data could be processes by *p*DISOL-X. The formula for acids in Table 2 predicted the $\wp$ value of saccharin to be 0.516. The product of $\wp N_{agg}$ suggested that n^{cof} = 32 (Eq. 14). From Eq. (13), the log K_n^{cof} was estimated as 58.9.

As the last step, the eight eutectic concentration data (in 22-400 mM SDS [9]) were subjected to a series of *p*DISOL-X analyses to determine the API and the coformer-micelle binding constant, following procedures described in detail elsewhere [16, 17]. The mean constants in the preceding paragraph were introduced as fixed parameters, and were not refined. The estimated K_n^{cof} constant indicated that the concentration of the saccharin-micelle species maximized at pH 1.7 but did not exceed 10^{-9} M; thus the constant was not subjected to refinement. Only log K_n was refined. The Appendix defines the function minimized and the goodness-of-fit (GOF) statistic.

The analysis of the Cao *et al.* data encountered an unexpected complication. The refined constant, K_n, depended critically on the actual weights of API and coformer added to the solutions. The original publication stated the quantities as ranges: 100-150 mg CC and 50-100 mg excess carbamazepine in 3 mL solution. Various combinations of weights were tried within/near the specified ranges. The minimum GOF 0.79 was found near 70 mg/mL CC + 35 mg/mL excess API. The refined constant, log K_{22} = 84.0, somewhat higher than the value obtained from non-CC data.

Figure 11 shows the eutectic curve and speciation plots for the cocrystal system for the $[SDS]_{tot}$ of 0, 22, 44, 250, and 400 mM. It was a complicated calculation. In frames (a)-(c)/(f)-(h), eutectic conditions hold up to pH 3, above which, the cocrystal dissolves but carbamazepine precipitate persists. Up to 44 mM SDS, the coformer eutectic curves are relatively unchanged, as the API curves are lifted by the added SDS, creating cross-over points in frames (b) and (c) at pH 1.7 and 2.2, respectively. At the two highest SDS concentrations, the cross-over is no longer evident, and even the coformer eutectic curves show upward lift (suggesting coformer-micelle complexes play a role). The 250 mM SDS is sufficient to dissolve the excess API at low pH, to form a "eutectoid" state (only CC precipitates; *cf.* Glossary), but only up to pH 2.69 (Fig. 11i). Between pH 2.69 and 2.90, a narrow eutectic state is predicted to form, as the SDS cannot suppress some API from precipitating. Above pH 2.9, the API remains the only residual solid in the suspension, as all of the CC dissolves. At the highest SDS concentration, the API is entirely micellized across the whole pH range. The eutectoid zone is thermodynamically stable up to pH 2.32, above which all solids dissolve (Fig. 11j). The same sample weights and the same equilibrium constants were used for all of the SDS-containing solutions.

Atazanavir:Pterostilbene 1:1 Cocrystal – Exploratory Simulation of an Unmeasured System

Given that one can predict k and K_{sp}^{CC}, it was of interest to consider if a cocrystal between atazanavir and pterostilbene could form. There are no reports of such a system in the literature. Two main sets of conditions were explored in the simulated data: atazanavir cocrystal added to solution with and without excess drug. In each case, 0, 10, and 20 mM $[SDS]_{tot}$ were part of the simulation compositions. The equilibrium constants (37 °C) used in the calculations are listed in Figure 12a. The pK_a and S_0 were determined by analysis of the atazanavir-SDS data from Indulkar *et al.* [20]. The pterostilbene S_0 was determined from data in [65], using the pK_a^{cof} estimated from 2D structure. Cocrystal K_{sp} was estimated by the method described elsewhere [17]. K_n was estimated by Eq. (13). In the simulations in Figure 12, all cases were based on 100 mg/mL CC added to water, with pH adjusted using either 1 M HCl or NaOH. In the Figure 13 cases, excess API, 50 mg/mL, was added to the simulated solutions, in addition to the 100 mg/mL CC.

Figure 12a shows the predicted eutectoid-eutectic concentration curves for the system in the absence surfactant. Below pH 3.23, the system is thermodynamically stable as a eutectoid (*cf.*, Glossary). The eutectoid

concentration of atazanavir is lower than that found in non-CC systems. That of the pterostilbene is largely elevated from its non-CC value. Above pH 3.23, the cocrystal system unstitches into non-equivalent eutectic API and coformer concentrations, with the API taking on the thermodynamic values observed in the non-CC system. Concomitantly, API precipitates. The thick dashed purple, marking S_{CC}, suggests an enhanced, albeit transient, concentration of the API. Adding the SDS, as in frames (b) and (c) has the effect of "zippering" the eutectic to a eutectoid state, to pH 8.62 in the case of 10 mM SDS and 9.79 in the case of 20 mM SDS. This has the effect of re-dissolving the API solid precipitated in the absence of the surfactant.

Figure 13 shows the simulated atazanavir:pterostilbene system where the CC is added along with an excess of API. The main effect is to "unzipper" the eutectoid states suggested in Figure 12. The middle-pH region in Figure 13b is nearly eutectoid, but not precisely so.

The simulations in the above two figures illustrate the kind of exploratory investigations that can be performed quickly *in silico*, as part of a plan to investigate a potential cocrystal system.

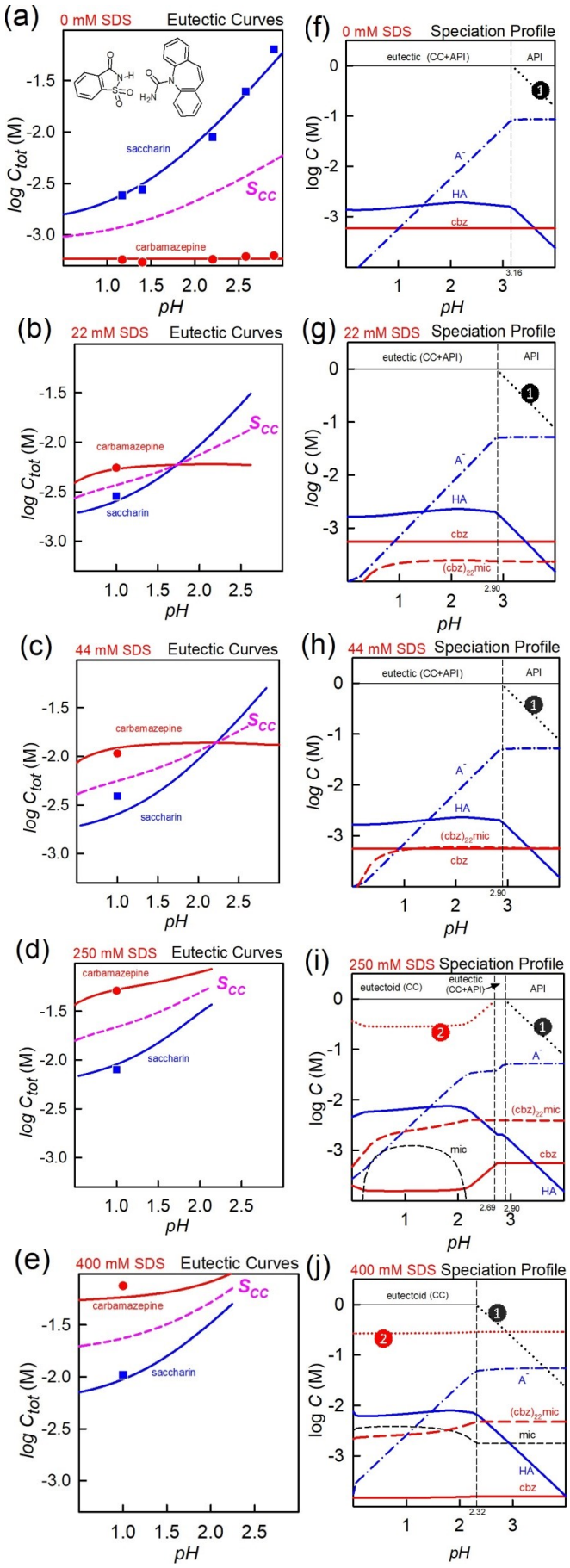

Figure 11. Carbamazepine:saccharin 1:1 cocrystal (data points from [9] and [64]). In all cases, the added CC and excess API weights were assumed to be 70 mg/mL and 35 mg/mL, respectively. The constants used (25 °C, I_{ref} = 0.2 M) were: pK_a^{cof} = 1.31, log K_{sp} = -6.01, log S_0 = -3.26, log K_{32}^{cof} = 58.9, and log K_{22} = 84.0. (a)-(e): The log C_{tot}-pH profiles as thick solid red ($[API]_{tot}$) and blue ($[cof]_{tot}$) curves refer to the calculated (best-fit) total aqueous concentrations in saturated solutions containing increasing concentrations of SDS. The symbols: red circle ($[API]_{tot,eu}$) and blue square ($[cof]_{tot,eu}$) refer to the reported eutectic total concentrations [9, 64]. The thick dashed purple curve (bounded by the API and coformer curves) refers to the calculated SCC. (f)-(j): The log speciation-pH profiles relate the concentrations of various (reactant and product) species to pH. The color assignments are the same as before. The thick solid curves refer to the carbamazepine (log $[API_0]$) and the uncharged form of saccharin (log $[cof_0]$). The corresponding charged forms are indicated by dash-dot curves. The vertical dashed lines mark cocrystal pH boundaries of the eutectic and eutectoid zones. The dotted curves ascending/descending from log C = 0 upper limit, indicated by black ❶ in the case of the CC and red ❷ in the case of the API, are computational "virtual" concentrations of solid, a tracking tool designed to anticipate the approach to the onset of a new precipitate (as log C ascends to 0), or the complete dissolution of a solid (as the virtual log C descends from 0)

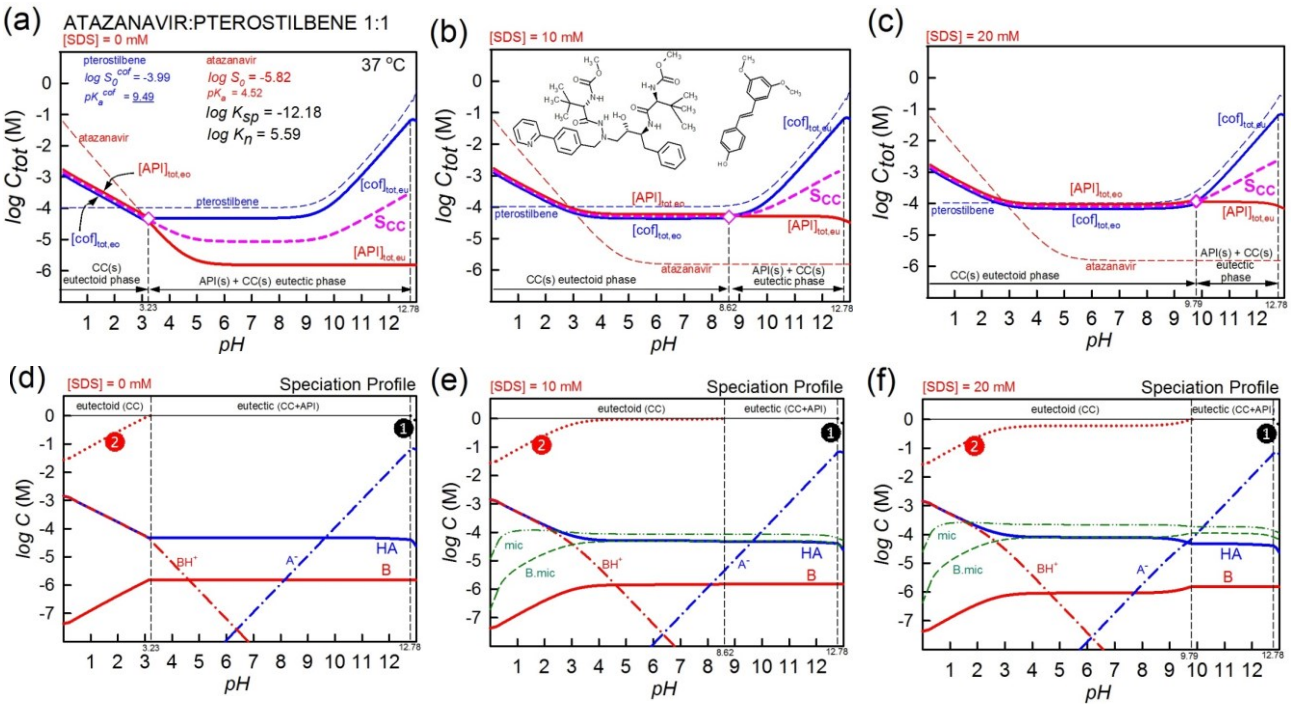

Figure 12. Hypothetical atazanavir:pterostilbene 1:1 cocrystal system simulated in the study, where 100 mg/mL cocrystal are added to an aqueous solution containing 0, 10, and 20 mM SDS. The symbols and curves are defined in Figure 11. The upper thin blue dashed curve refers to the log *S*-pH profile expected of pterostilbene in absence of the API, and is calculated using the Henderson-Hasselbalch equation. The lower thin red dashed curve refers to the log *S*-pH profile expected of atazanavir in absence of the coformer.

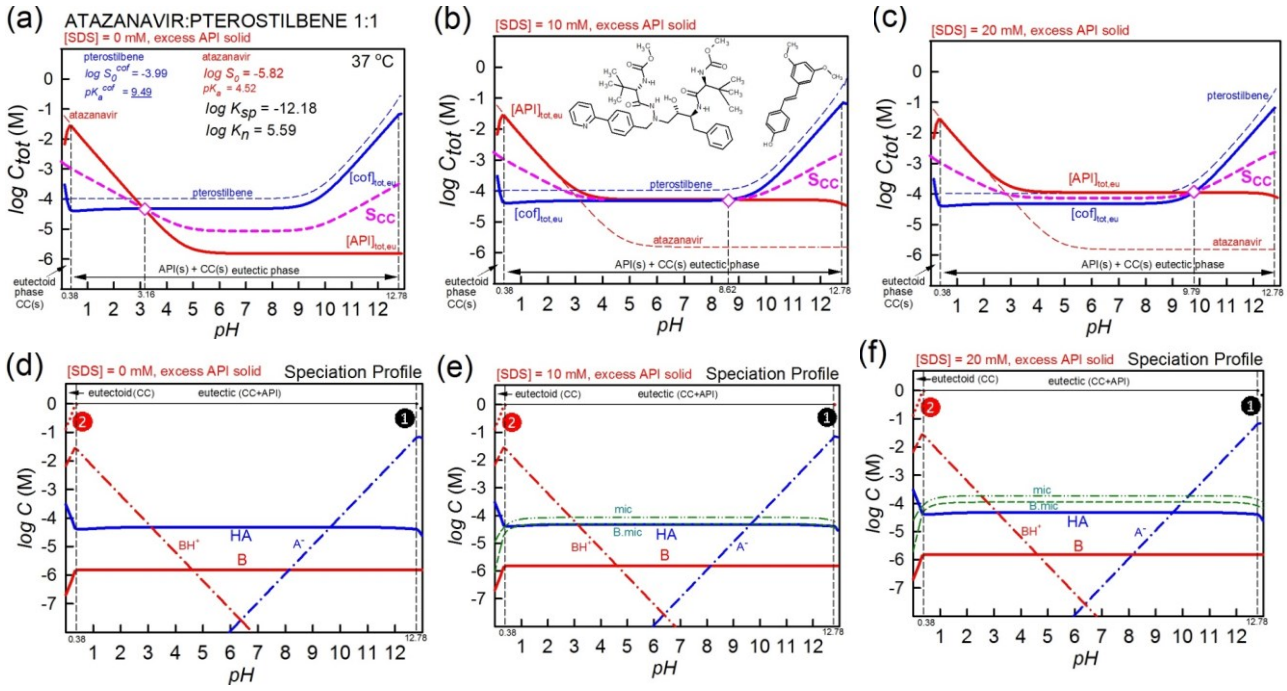

Figure 13. Hypothetical atazanavir:pterostilbene 1:1 cocrystal system simulated in the study, the same system as in Figure 12, except that 100 mg/mL cocrystal plus 50 mg/mL atazanavir are added to aqueous solutions containing 0, 10, and 20 mM SDS.

Summary

This review considered the uses of the anionic surfactant, sodium dodecyl sulfate (SDS), to mitigate poor bioavailability of some drugs due to their low aqueous solubility. A small database of 101 drug solubilizing capacity (κ) values was compiled from published sources, from which a κ predictive model was derived. The mass action paradigm was used to describe drug-micelle equilibrium reactions in aqueous-micellar-solid media, as a function of pH, ionic strength, and quantities of reactants used. The κ values were converted to drug-micelle stoichiometric binding constants, K_n, corresponding to drug-micelle equilibria in drug-saturated solutions, with n values (Table 1) ranging from 1 (*e.g.*, practically-insoluble drugs: atazanavir, clofazimine, glibenclamide, mefenamic acid) to over 50 (*e.g.*, small substituted benzoic acids, ketoprofen, 3-toluic acid). The K_n values were further refined by generalized regression analysis in select cases. In the absence of drug, the monomer-micelle cumulative equilibrium, $62\ SDS^- + 50\ Na^+ \leftrightarrows SDS_{62}Na_{50}^{12-}$, was consistent with the critical micelle concentration (CMC) of 8.3 mM for the aggregation constant log K_{SDS} = 230.6. Also, this constant correctly predicted the CMC values as a function of added NaCl. The effect of drug on the above equilibrium was considered in select cases. An in-depth case study of the weak base, PG-300995 [24, 49, 60], considered the micellization reactions as a function of pH. At pH 1 the drug-SDS salt was predicted to precipitate both below and above the CMC. At very low SDS concentrations, the chloride salt was predicted to co-precipitate with the drug-SDS salt. Both solubility products were determined in the analysis of the reported solubility-surfactant data. Above the CMC, in a rare example, the *charged* form of the drug was strongly solubilized: $4\ BH^+ + SDS_{62}Na_{50}^{12-} \leftrightarrows (BH)_4SDS_{62}Na_{50}^{8-}$, with the estimated binding constant, log K_n = 23.0. At pH 7, only the neutral form of the drug was solubilized, with log K_n = 7.4 (n=2). Also considered were examples of solubilization of solids in the form of cocrystals. The case studies included the carbamazepine:saccharin system, whose experimental data were analyzed to determine the binding constants. A recently-described method for predicting the solubility product of cocrystals (coupled with predicted κ values described here) allowed for simulations of solubility-pH speciation profiles of cocrystal systems in the presence of SDS. Purely on *in silico* grounds, atazanavir was postulated to form a cocrystal with pterostilbene. This remains to be validated experimentally. Data patterns depending on the amount of SDS added and the extent of drug excess over the cocrystal amount added to solution were explored *in silico*.

Conclusion

The main objective of the study was to apply simulation methods to represent drug-micelle equilibrium reactions (based on the mass action paradigm), so as to optimize the design of experimental approaches used to assess drug solubility as a function of pH and the amount of added sodium dodecyl sulfate, particularly when applied to cocrystal formulations. In this endeavor, a new prediction model for the drug solubilization capacity (κ) of sodium dodecyl sulfate was described. Well in advance of any actual measurements, these simulations can be used to probe conditions favorable to the design of experiments where SDS can stabilize cocrystal suspensions against drug precipitation over a range of pH values, in an effort to improve the rate and extent of oral absorption of the drug.

Glossary

API	active pharmaceutical ingredient, *i.e.*, the 'drug' molecule
coformer	"generally regarded as safe" soluble molecule that can combine with an API to form a cocrystal
$[API_0]$ ($[cof_0]$)	concentration of the neutral form of API (or coformer) determined from eutectic and/or eutectoid data
$[API]_{tot,eu(eo)}$	measured equilibrium total aqueous concentration of the API at a eutectic (or eutectoid) point in a solution with a particular pH; *e.g.*, points indicated as red circles in Figs. 3-5
$[cof]_{tot,eu(eo)}$	measured equilibrium total aqueous concentration of the coformer at a eutectic (or eutectoid) point with a particular pH; *e.g.*, points indicated as blue squares in Figs. 3-5
eutectic (eu)	3-phase system comprising a stable suspension containing both CC and crystalline API (or coformer) in contact with a saturated aqueous solution with both API- and coformer-containing species at a particular pH
eutectoid (eo)	"sub-eutectic" point with thermodynamically stable CC and suppressed API and coformer precipitation: 2 phase system comprising a stable suspension containing just the CC in contact with a saturated aqueous solution with both API- and coformer-containing species at a particular pH; system may form even when CC plus API/coformer solids are added to water
SDS (SLS)	sodium dodecyl sulfate (*i.e.*, sodium lauryl sulfate)
CMC	critical micelle concentration
N_{agg}	micelle aggregation number (62 for SDS is assumed)
N_d	average number of bound drugs per micelle
f_{bm}	fraction of drug-bound micelles
K_n	drug-micelle binding constant, where n drugs are bound to one micelle
K_{SDS}	micelle aggregation constant (*cf.*, Eq. 1)
S	solubility, ideally expressed in units of mol/L (M) or mg/mL
S_0	"intrinsic" solubility (*i.e.*, the solubility of the *uncharged* form of the compound)
S_w	"water" solubility, defined by dissolving enough pure free acid/base (not drug salt) in water (or water containing an inert salt - as ionic strength adjustor) to form a saturated solution
S_{CC}	solubility of CC; if a eutectoid system forms by adding excess CC (without additional API or coformer) to pH-adjusted water, then $S_{CC} = [API]_{tot,eo} = [cof]_{tot,eo}$; *e.g.*, curves indicated by purple thick dashed lines in Figs. 11-13.
S_0^{API} (S_0^{cof})	intrinsic solubility in a non-CC 2-phase system, where the crystalline API (or coformer) is in equilibrium with a saturated solution of the neutral API (or coformer)
$\Sigma\alpha_2^H$	Abraham descriptor – solute H-bond total acidity (also called A)
$\Sigma\beta_2^H$	Abraham descriptor – solute H-bond total basicity (also called B)
π_2	Abraham descriptor – solute polarity/polarizability due to solute-solvent interactions between bond dipoles and induced dipoles (also called S)
R_2	Abraham descriptor – excess molar refraction ($L \cdot mol^{-1}$ / 10); which models dispersion force interaction arising from pi- and n-electrons of the solute (also called E)
V_x	Abraham descriptor – McGowan molar volume ($L \cdot mol^{-1}$ / 100) of the solute
I_A, I_B, I_{AB}, I_N	indicator indices: unit value, indicating that a molecule is an acid, base, ampholyte, or neutral, respectively, and zero otherwise

Acknowledgements

Helpful discussions with Profs. Naír Rodríguez-Hornedo (Univ. of Michigan, USA) and Elena Boldyreva (Institute of Solid State Chemistry and Mechanochemistry, Novosibirsk, Russian Federation) on the topic of cocrystals are much appreciated.

References

[1] S.R. Burn, G. Zografi, X.S. Chen. *Solid-state Properties of Pharmaceutical Materials*. John Wiley & Sons, Inc., Hoboken, NJ, 2017.

[2] H.G. Brittain. Cocrystal systems of pharmaceutical interest: 2011. *Cryst Growth Des.* **12** (2012) 5823-5832.

[3] J. Wouters, L. Quéré (Eds.). *Pharmaceutical Salts and Co-crystals*. Royal Society of Chemistry, Cambridge, 2012.

[4] J.W. Steed. The role of co-crystals in pharmaceutical design. *Trends Pharm Sci.* **34** (2013) 185-193.

[5] G. Kuminek, F. Cao, A. Bahia de Oliveira da Rocha, S.G. Cardoso, N. Rodríguez-Hornedo. Cocrystals to facilitate delivery of poorly soluble compounds beyond-rule-of-5. *Adv. Drug Deliv. Rev*. **101** (2016) 143-166.

[6] N. Huang, N. Rodríguez-Hornedo. Engineering cocrystal solubility, stability, and pH_{max} by micellar solubilization*. J. Pharm. Sci.* **100** (2011) 5219-5234.

[7] I. Tomaszewska, S. Karki, J. Shur, R. Price, N. Fotaki. Pharmaceutical characterisation and evaluation of cocrystals: importance of *in vitro* dissolution conditions and type of coformer*. Int. J. Pharm*. **453** (2013) 380-388.

[8] M.P. Lipert, L. Roy, S.L. Childs, N. Rodriguez-Hornedo. Cocrystal solubilization in biorelevant media and its prediction from drug solubilization. *J. Pharm. Sci*. **104** (2015) 4153–4163.

[9] F. Cao, G.L. Amidon, N. Rodríguez-Hornedo, G.E. Amidon. Mechanistic analysis of cocrystal dissolution as a function of pH and micellar solubilization. *Mol. Pharmaceutics*. **13** (2016) 1030-1046.

[10] Y. He, S. H. Yalkowsky. Solubilization of monovalent weak electrolytes by micellization or complexation. *Int. J. Pharm*. **314** (2006) 15–20.

[11] A.T. Florence, D. Attwood. *Physicochemical Principles of Pharmacy – in Manufacture, Formulation and Clinical Use*. 6th Ed., Pharmaceutical Press, London, 2016, pp. 193-245.

[12] E. Pramauro, E. Pelizzetti. *Surfactants in Analytical Chemistry – Applications of Organized Amphiphilic Media*. Elsevier, Amsterdam, 1996.

[13] M. Žegarac, E. Lekšić, P. Šket, J. Plavec, M.D. Bogdanović, D.-K. Bučar, M. Dumić, E. Meštrović. A sildenafil cocrystal based on acetylsalicylic acid exhibits an enhanced intrinsic dissolution rate. *Cryst. Eng. Comm.* **16** (2014) 32-35.

[14] K.J. Box, J. Comer, R. Taylor, S. Karki, R. Ruiz, R. Price, N. Fotaki. Small-scale assays for studying dissolution of pharmaceutical cocrystals for oral administration. *AAPS PharmSciTech*. **17** (2016) 245-251.

[15] D.P. McNamara, S.L. Childs, J. Giordano, A. Iarriccio, J. Cassidy, M.S. Shet, R. Mannion, E. O'Donnell, A. Park. Use of a glutaric acid cocrystal to improve oral bioavailability of a low solubility API. *Pharm. Res*. **23** (2006) 1888-1897.

[16] A. Avdeef. Cocrystal solubility product analysis – dual concentration-pH mass action model not dependent on explicit solubility equations. *Eur. J. Pharm. Sci.* **110** (2017) 2-18.

[17] A. Avdeef. Cocrystal solubility product prediction using an *in combo* model and simulations to improve design of experiments. *Pharm. Res.* (2018) 35: 40. https://doi.org/10.1007/s11095-018-2343-3.

[18] E. Fuguet, C. Ràfols , M. Rosés, E. Bosch. Critical micelle concentration of surfactants in aqueous buffered and unbuffered systems. *Anal. Chim. Acta* 548 (2005) 95–100.

[19] A.M. Khan, S.S. Shah. Determination of critical micelle concentration (CMC) of sodium dodecyl sulfate (SDS) and the effect of low concentration of pyrene on its CMC using ORIGIN software. *J.Chem.Soc. Pak*. 30 (2008) 186-191.

[20] A.S. Indulkar, H. Mo, Y. Gao, S.A. Raina, G.G.Z. Zhang, L.S. Taylor. Impact of micellar surfactant on supersaturation and insight into solubilization mechanisms in supersaturated solutions of atazanavir. *Pharm. Res.* 34 (2017) 1276–1295.

[21] G. Völgyi, A. Marosi, K. Takács-Novák, A. Avdeef. Salt Solubility Products of Diprenorphine Hydrochloride, Codeine and Lidocaine Hydrochlorides and Phosphates – Novel Method of Data Analysis Not Dependent on Explicit Solubility Equations. *ADMET & DMPK* **1** (2013) 48-62.

[22] A. Avdeef. Anomalous Solubility Behavior of Several Acidic Drugs. *ADMET & DMPK* **2** (2014) 33-42.

[23] A. Avdeef. Phosphate Precipitates and Water-Soluble Aggregates in Re-examined Solubility-pH Data of Twenty-five Basic Drugs. *ADMET & DMPK* **2** (2014) 43-55.

[24] G. Butcher, J. Comer, A. Avdeef. pK_a-critical Interpretations of solubility-pH profiles: PG-300995 and NSC-639829 case studies. *ADMET & DMPK* **3** (2015) 131-140.

[25] A. Pobudkowska, C. Ràfols, X. Subirats, E. Bosch, A. Avdeef. Phenothiazines solution complexity – determination of pK_a and solubility-pH profiles exhibiting sub-micellar aggregation at 25 and 37 ^{o}C. *Eur. J. Pharm. Sci*. **93** (2016) 163-176.

[26] A. Avdeef. Solubility temperature dependence predicted from 2D structure. *ADMET & DMPK* **3** (2015) 298-344.

[27] A. Avdeef. *Absorption and Drug Development,* Second Edition. Wiley-Interscience, Hoboken, NJ, 2012.

[28] S. Lapenna S, A.R. Bilia, G.A. Morris, M. Nilsson M. Novel Artemisinin and curcumin micellar formulations: drug solubility studies by NMR spectroscopy. *J. Pharm. Sci.* **98** (2009) 3666-367515.

[29] A.S. Indulkar, H. Mo, Y. Gao, S.A. Raina, G.G.Z. Zhang, L.S. Taylor. Impact of Micellar Surfactant on Supersaturation and Insight into Solubilization Mechanisms in Supersaturated Solutions of Atazanavir. *Pharm. Res*. **34** (2017) 1276–1295.

[30] K.M.S. Fahelelbom, R.F. Timoney, O.I. Corrigan. Micellar solubilization of clofazimine analogues in aqueous solutions of ionic and nonionic surfactants. *Pharm. Res*. **10** (1993) 631-634.

[31] A. Garrone, E. Marengo, E. Fornatto, A. Gasco. A study on pK_a^{app} and partition coefficient of substituted benzoic acids in SDS anionic micellar system. *Quant. Struct.-Act. Relat*. **11** (1992) 171-175.

[32] J.R. Crison, V.P. Shah, J.P. Skelly, G.L. Amidon. Drug dissolution into micellar solutions: development of a convective diffusion model and comparison to the film equilibrium model with application to surfactant-facilitated dissolution of carbamazepine. *J. Pharm. Sci.* **85** (1996) 1005-1011.

[33] M. Li, N. Qiao, K. Wang. Influence of sodium lauryl sulfate and Tween 80 on carbamazepine–nicotinamide cocrystal solubility and dissolution behaviour. *Pharmaceutics* **5** (2013) 508-524.

[34] N. Ni, T. Sanghvi, S.H. Yalkowsky. Solubilization and preformulation of carbendazim. *Int. J. Pharm*. **244** (2002) 99–104.

[35] S. Chakraborty, D. Shukla, A. Jain, B. Mishra, S. Singh. Assessment of solubilization characteristics of different surfactants for carvedilol phosphate as a function of pH. *J. Colloid Inter. Sci*. **335** (2009) 242–249.

[36] S. Feng. Studies on drug solubilization mechanism in simple micelle systems. Ph.D. Thesis, Univ. Kentucky, 2009.

[37] P.A. Bhat, A.A. Dar, G.M. Rather. Solubilization capabilities of some cationic, anionic, and nonionic surfactants toward the poorly water-soluble antibiotic drug erythromycin. *J. Chem. Eng. Data* **53** (2008) 1271–1277.

[38] S. Jamzad, R. Fassihi. Role of surfactant and pH on dissolution properties of fenofibrate and glipizide—a technical note. *AAPS PharmSciTech* **7** (2006) E1-E6.

[39] N. Seedher, M. Kanojia. Micellar solubilization of some poorly soluble antidiabetic drugs: a technical note. *AAPS PharmSciTech* **9** (2008) 431-436.

[40] K.A. Johnson, G.B. Westerman-Clark, D.O. Shah. Transport of micelle-solubilized steroids across microporous membranes. *J. Pharm. Sci*. **76** (1987) 277-285.

[41] S.-H. Park, H.-K. Choi. The effects of surfactants on the dissolution profiles of poorly water-soluble acidic drugs. *Int. J. Pharm*. **321** (2006) 35–41.

[42] C.O. Rangel-Yagui , H.W.L. Hsu, A. Pessoa, Jr., L.C. Tavares. Micellar solubilization of ibuprofen – influence of surfactant head groups on the extent of solubilization. *Brazilian J. Pharm. Sci.* **41** (2005) 237-246.

[43] S.D. Bhattamishra, R.K. Padhy. Estimation of ibuprofen solubilization in cationic and anionic surfactant media: application of micelle binding model. *Indian J. Chem. Tehnol*. **16** (2009) 426-430.

[44] D. Bolten, R. Lietzow, M. Türk. Solubility of ibuprofen, phytosterol, salicylic acid, and naproxen in aqueous solutions. *Chem. Eng. Technol*. **36** (2013) 426–434.

[45] N.M. Najib, M.S. Suleiman. The effect of hydrophilic polymers and surface active agents on the solubility of indomethacin. *Int. J. Pharm*. **24** (1985) 165-171.

[46] J.J. Sheng, N.A. Kasim, R. Chandrasekharan, G.L. Amidon. Solubilization and dissolution of insoluble weak acid, ketoprofen: effect of pH combined with surfactant. *Eur. J. Pharm. Sci.* **29** (2006) 306-314.

[47] G. Popović, M. Čakar, D. Agbaba. Acid–base equilibria and solubility of loratadine and desloratadine in water and micellar media. *J. Pharm. Biomed. Anal*. **49** (2009) 42-47.

[48] G. Yang, N. Jain, S.H. Yalkowsky. Combined effect of SLS and $(SBE)_{7M}$-β-CD on the solubilization of NSC-639829. *Int. J. Pharm*. **269** (2004) 141–148.

[49] A. Jain, Y. Ran, S.H. Yalkowsky. Effect of pH-sodium lauryl sulfate combination on solubilization of PG-300995 (an anti-HIV agent): a technical note. *AAPS PharmSciTech* **5** (2004) 1-3 (article 45).

[50] K. Kawakami , N. Oda, K. Miyoshi, T. Funaki, Y. Ida. Solubilization behavior of a poorly soluble drug under combined use of surfactants and cosolvents. *Eur. J. Pharm. Sci*. **28** (2006) 7-14.

[51] J. Jinno, D.-M. Oh, J.R. Crison, G.L. Amidon. Dissolution of ionizable water-insoluble drugs: the combined effect of pH and surfactant. *J. Pharm. Sci*. **89** (2000) 268-274.

[52] J. Cvejić, M. Poša, A. Sebenji, M. Atanacković. Comparison of solubilization capacity of resveratrol in sodium 3α,12α-dihydroxy-7-oxo-5β-cholanoate and sodium dodecyl sulfate. *Sci. World J.,* vol. 2014, Article ID 265953, 7 pages, doi.org/10.1155/2014/265953.

[53] L. Stopková, A. Hriňaková, Ž. Bezáková, J. Oremusová, F. Andriamanty, V. Žufková. Influence of valsartan on the thermodynamics of micellization of anionic surfactant sodium dodecyl sulphate. *Eur. Pharm. J*. **63** (2016) 30-36.

[54] S.H. Yalkowsky, Y. He, P. Jain. *Handbook of Aqueous Solubility Data*. Second Edition. CRC Press - Taylor & Francis Group, Boca Raton, FL, 2010.

[55] A. Avdeef. Suggested improvements for measurement of equilibrium solubility-pH of ionizable drugs. *ADMET & DMPK* **3** (2015) 84-109.

[56] A. Avdeef, E. Fuguet, A. Llinàs, C. Ràfols, E. Bosch, G. Völgyi, T. Verbić, E. Boldyreva, K. Takács-Novák. Equilibrium solubility measurement of ionizable drugs – consensus recommendations for improving data quality. *ADMET & DMPK* **4** (2016) 117-178.

[57] N. Sun, A. Avdeef. Biorelevant pK_a (37°C) Predicted from the 2D Structure of the Molecule and its pK_a at 25 °C. *J. Pharm. Biomed. Anal.* **56** (2011) 173-182.

[58] M.H. Abraham, H.S. Chadha, J.P. Dixon, C. Ràfols, C. Treiner. Hydrogen bonding. Part 40. Factors that influence the distribution of solutes between water and sodium dodecyl sulfate micelles. J . *Chem. Soc. Perkin Trans. 2* (1995) 887-894.

[59] M.H. Abraham. Scales of hydrogen bonding - their construction and application to physicochemical and biochemical processes. *Chem. Soc. Revs*. **22** (1993) 73-83.

[60] Y. Ran, A. Jain, S.H. Yalkowsky. Solubilization and preformulation studies on PG-300995 (an anti-HIV drug). *J. Pharm. Sci.* **94** (2005) 297-303.

[61] C. Stubbs, I. Kanfer. A stability indicating high-performance liquid chromatographic assay of erythromycin estolate in pharmaceutical dosage forms. *Int. J. Pharm*. **63** (1990) 113-119.

[62] D.J. Good, N. Rodríguez-Hornedo. Solubility advantage of pharmaceutical cocrystals. *Cryst. Growth Des.* 9 (2009) 2252-2264.

[63] N.C. Huang. Engineering cocrystal solubility and stability via ionization and micellar solubilization. PhD Thesis, University of Michigan, 2011.

[64] A. Alhalaweh, L. Roy, N. Rodríguez-Hornedo, S.P. Velaga. pH-dependent solubility of indomethacin-saccharin and carbamazepine-saccharin cocrystals in aqueous media. *Mol. Pharmaceutics*. 9 (2012) 2605-2612.

[65] N. Schultheiss, S. Bethune, J.-O. Henck. Nutraceutical cocrystals: utilizing pterostilbene as a cocrystal former. *CrystEngComm*. **12** (2010) 2436–2442.

Appendix. Function Minimized in Refinement of Cocrystal Solubility Products and Drug-Surfactant Binding Constants

Function Minimized in the Weighted Nonlinear Regression Analysis

The refined equilibrium constants (drug-micelle binding constant, K_n, cocrystal K_{sp} and API intrinsic solubility, S_0), along with other unrefined constants (e.g., API and coformer pK_a values), and the given independent variables (sample weights, reagent volumes, surfactant concentration, etc.), are used to calculate the dependent variables: the eutectic/eutectoid total concentrations of the API (general symbol X_{tot}) and the coformer (general symbol Y_{tot}). The calculated total concentrations are then compared to the corresponding observed values at each measured pH. The refined 'best' values are those which produce a minimum in the sums of the weighted squares of two sets of residuals,

$$R_w = \sum_i^{N_o}\left(\frac{\log X_{tot,i}^{obs} - \log X_{tot,i}^{calc}}{\sigma_i(\log X_{tot,i}^{obs})}\right)^2 + \sum_i^{N_0^{cof}}\left(\frac{\log Y_{tot,i}^{obs} - \log Y_{tot,i}^{calc}}{\sigma_i(\log Y_{tot,i}^{obs})}\right)^2 \quad \text{(A.1)}$$

N_0 and N_0^{cof} are the number of API and coformer measurements as a function of pH, respectively; σ is the estimated standard deviation in the measured log value. (When σ values were not available, 0.1 log unit was assumed.) X_{tot}^{calc} and Y_{tot}^{calc} are functions of the equilibrium constants, as well as the independent variables.

Overview of the refinement procedure

Two separate stages of refinement comprise the overall procedure.

(i) At the 'local' refinement stage (pp. 152-154 [27]), the mass balance equations (e.g., Eqs. (8)-(10)), which are nonlinear polynomials in terms of the reactant concentrations and equilibrium constants, are simultaneously solved by the Jacobian method for reactant concentrations at each measured solubility point, for a given set of equilibrium constants. If there are three independent reactants, then there will be three mass balance equations. The local step involves the inversion of a symmetric Jacobian matrix (whose elements are partial derivatives of total concentrations as a function of the logarithmic reactant concentrations) at each observed eutectic/eutectoid-pH measurement. If solids are part of the system, then the computation of the reactant concentrations becomes quite complicated, as described in detail elsewhere [16].

(ii) At the 'global' stage of refinement (pp. 154-155 [27]), the Gauss-Newton method is used to approximate the log C_{tot} values (based on the mass balance equations) by 'normal equations' (one for each sampled log C_{tot}-pH), linearized by Taylor series expansion. The least-squares symmetric matrix (of dimension equal to the number of refined parameters) to be inverted will have its elements computed from the first derivatives of log C_{tot}^{calc} with respect to the adjustable parameters (related to the 'local' inverse Jacobian matrix). The partial derivatives are computed at the 'local' refinement steps and elements of the global design matrix are accumulated for each pH point. When all the data points have been processed, the accumulated matrix is inverted and the newly-estimated equilibrium constants are incrementally calculated. The iterative process continues until the improvements are vanishingly small.

Weighting scheme and goodness-of-fit, GOF

After each global iterative cycle, the progress of refinement is indicated by the 'goodness-of-fit', GOF, as

$$GOF = \sqrt{\frac{R_w}{N_0 + N_0^{cof} - N_v}} \quad \text{(A.2)}$$

where N_v is the number of varied equilibrium constants. GOF values of 1 are ideal. It would mean that on the average, the calculated and observed log C_{tot} - pH curves are about one standard deviation (0.05-0.1 log unit) apart. GOF 0.5-1.5 is often obtained for successful refinement. GOF >> 2 indicates that log C_{tot} measurements are of poor quality, or the experimental standard deviations are underestimated, or the assumed equilibrium model is incomplete or inappropriate.